

Excitation and Guiding of Surface Plasmon Polaritons by  
Arrays of Metal NanoParticles

P. J. Compaijen

Supervisors: Dr. V. A. Malyshev and Prof. dr. J. Knoester

July 29, 2011

## Abstract

The possibility of extending the propagation length of electromagnetic fields by placing an array of metal nanoparticles close to a dielectric metal interface. We have considered silver nanospheres (radius 50 nm) embedded in a dielectric ( $\epsilon = 2.25$ ) in the proximity of a perfect reflector and of a silver halfspace. We calculated that the presence of a perfect reflector has a positive influence on the propagation length of the electric field through the chain. Considering silver instead of a perfect reflector, gives the possibility of exciting surface plasmon polariton (SPP) modes. These mode extend the propagation length further, depending on how the wavelength of these modes matches with the inter-particle spacing in the array. Furthermore, a method to analytically calculate the SPP contribution to the electric field is proposed and it was shown that these modes give the major contribution to the total field on the interface. This opens up the possibility for a quick and analytical algorithm for the calculation of the electric field in these systems.

# Contents

<b>1</b>	<b>Introduction</b>	<b>3</b>
<b>2</b>	<b>Theory</b>	<b>6</b>
2.1	Surface Plasmon Polaritons from Maxwell's equations . . . . .	6
2.1.1	Maxwell's equations on the interface between two media . . . . .	6
2.1.2	Properties of SPPs . . . . .	10
2.2	Response of a Metal Nanosphere to an Oscillating Electric Field . . . . .	15
2.3	An oscillating dipole close to an interface . . . . .	17
2.3.1	Deriving the equations for the electric field . . . . .	17
2.3.2	Coupling to SPP modes . . . . .	26
2.3.3	Calculating the Sommerfeld-integrals . . . . .	27
2.4	Green's tensor formalism . . . . .	32
<b>3</b>	<b>Results and Discussion</b>	<b>35</b>
3.1	One metal nanoparticle close to a metal half-space . . . . .	35
3.2	An array of metal nano-particles close to a metal surface . . . . .	42
3.2.1	Dipole moments of metal nano-particles in an array close to an interface . . . . .	42
3.2.2	Electric field produced by an array of metal nano-particles . . . . .	50
<b>4</b>	<b>Conclusion and Suggestions for further research</b>	<b>55</b>
4.1	Excitation of SPP-modes by a single Metal Nanoparticle . . . . .	55
4.2	Energy transport through an array of Metal Nanoparticles in the proximity of an interface . . . . .	56
4.3	Guiding of SPP-modes by an array of Metal Nanoparticles . . . . .	57
4.4	Suggestions for further research . . . . .	57

---

<b>A Equations for the electric field produced by a driven dipole oscillator close to an interface</b>	<b>59</b>
A.1 Definitions . . . . .	59
A.2 The Hertz vector potentials . . . . .	60
A.3 Dipole oscillating perpendicular to the interface . . . . .	61
A.4 Dipole oscillating parallel to the interface in the x-direction . . . . .	62
A.5 Dipole oscillating parallel to the interface in the y-direction . . . . .	63

# Chapter 1

## Introduction

To increase speed and bandwidth for on-chip communication, it would be very convenient to make use of the high velocity and frequency of light. However, present day photonic chips have a footprint of at least one square centimeter, whereas electronic components can already be build at the nanometer scale. This size-mismatch makes it critical for photonic components to be scaled down to the nanometer regime.

A fast developing field that explores how electromagnetic fields can be confined to sizes smaller than the wavelength, is called plasmonics. Using plasmons, which are collective excitations of free electrons in a metal, it is possible to manipulate and guide light well below the diffraction limit [1]- [13]. Of specific interest for guiding purposes are the so-called surface plasmon polaritons (SPPs), i.e. coupled excitations of plasmons and photons on the interface between a metal and a dielectric.

The first study of surface bound electromagnetic modes dates back to the work Zenneck [15] and Sommerfeld [14] performed (independently) on the radiation of radio antennas close to the earth. These waves were studied in detail because of the possible relevance for the transmission of radio signals. Interest faded, when people realized that for radio communication the dominating process is the scattering at the ionosphere, instead transmission through surface modes. However, recent advances in nano-fabrication have made it possible to scale down these radio antennas to the optical regime and have brought new life to the study of bound surface modes. For the interface between a metal and a dielectric, these modes are identified as SPP modes.

A typical propagation length of SPPs in the visible regime is on the order of  $10 \mu m$  and the extension of the mode into the dielectric is on the order of 100 nm. The SPP-

mode extends around 20 nm into the metal. A trade-off that is typical for plasmonics, is that increasing the propagation length will lead to a poorer confinement to the interface. This implies that for matching plasmonics with nano-electronics, one should be able to somehow overcome this trade-off.

A possible way to solve this problem is by designing waveguides that are able to confine the SPPs, but at the same time reduce the losses [5], [16], [17]. It has been shown that for Metal-Insulator-Metal waveguides with a separation between the metal plates on the order of 100 nm, the only allowed mode is the SPP mode. This implies that most of the energy that is inserted, will be coupled into SPP modes. However, as we will be shown in section 2.1, it is not possible to excite SPP modes directly with light, but phase matching techniques (like gratings or prisms) are needed [1]. Another possibility is to excite SPP mode by using the near field of an oscillating dipole [2]. This can be e.g. an optically excited metal nanoparticle or an electronically excited quantum dot. Although the treatment for both of these particles is the same under weak excitation conditions, the latter has much more potential for use in opto-electronics because of the precise electronic excitation and the easier production.

Using oscillating dipoles for the excitation of SPP on the interface between a metal and a dielectric, rises the question of what will happen if an array of dipoles would be used instead of one. After exciting the first dipole of the array, a signal starts propagating along the array and along the interface. Each of the dipoles in the array can then excite new SPP modes on the interface, resulting in an extended propagation of the SPPs. Using this geometry, SPP propagation for over 120  $\mu\text{m}$  has been reported [11].

This geometry has been studied in detail in the research reported in this thesis. Throughout this research silver nanospheres with a radius of 50 nm are assumed. The first nanoparticle will be excited with continuous wave excitation. The response of the particles to the applied electric field is calculated in the quasi-static approximation, i.e. they are treated as point dipoles. For calculating the interactions between the individual particles and the interaction of the particles with the interface, the full field Green's tensors are used. This means that both the far field and the near field of the oscillating dipoles are taken into account and therefore, all particles interact. The electric field reflected from the interface is calculated using Sommerfelds method [14]. Using these methods a careful and detailed study of the important parameters in this geometry can be performed.

The uniqueness of this research is in the investigation of the influence of the center-

to-center distance of the particles in the array, the height of the array above the metal and the excitation wavelength on the energy propagating through the chain and the energy propagating over the interface. Furthermore, it will be shown that it is actually the SPP mode than gives the largest contribution to the guided electromagnetic field. Understanding the importance of these parameters will lead to a better understanding of the important interactions in the system and will be valuable for designing and applying these types of systems for sub-wavelength guiding of electromagnetic fields.

We will address three major topics:

1. The excitation of surface plasmon polaritons (SPPs) by a single metal nanoparticle (MNP) and the properties of these SPPs
2. The propagation of the electric field through an array of MNPs. First an isolated array will be considered. To find the influence of the presence of a reflecting interface, a perfect mirror will be placed in proximity. Finally, to investigate the influence of the SPP modes, the array will be placed near a silver halfspace
3. The propagation of the electric field at the interface, created by an array of MNPs positioned close to this interface.

In chapter 2, the theoretical model that we use will be outlined. First the general properties of SPPs will be derived from Maxwell's equations. Then we will describe how a MNP responds to an oscillating electric field. Using Sommerfeld's method, it will then be explained how the electric field of an oscillating dipole close to a partially reflecting interface can be calculated. The so-called Sommerfeld integrals will be derived and an clear explanation of how this integrals can be calculated, will be presented. Finally, using the Green's tensor formalism, the interactions between the MNPs will be derived.

The results of our calculations for the three cases mentioned above, will be discussed in chapter 3. In the last chapter, some conclusions will be drawn and suggestions for further research are given.

# Chapter 2

## Theory

In this chapter, we present the theoretical framework used in this project. To give a clear description, we divide the array of MNPs above a dielectric/metal interface into several subsystems. First, we study the physical properties of the bound surface wave solution to Maxwell's equations and how SPPs can be excited. After this, we will give a description of a MNP in an oscillating field. Knowing what SPPs are and how MNPs respond to an oscillating field, we will calculate the electric field produced by a MNP close to a metallic interface and the excitation of SPPs by this particle. To extend the treatment to an array of particles, we will use the Green's tensor formalism.

### 2.1 Surface Plasmon Polaritons from Maxwell's equations

Surface Plasmon Polaritons (SPPs) are a type of electromagnetic surface waves and therefore, they have to obey Maxwell's equations. Indeed, it is possible to find a solution to Maxwell's equations on the interface between a metal and a dielectric. In this section, we present the basic steps that need to be taken to find this solution. A more detailed procedure can be found in [1, ch. 2] or in [2, ch. 12]. After finding the solution, the physical properties of these surface modes will be discussed in detail.

#### 2.1.1 Maxwell's equations on the interface between two media

We start off with Maxwell's equations of macroscopic electromagnetism in the form as given in [19]:



$$\nabla \cdot \mathbf{D} = \rho, \quad (2.1.1)$$

$$\nabla \times \mathbf{H} - \frac{\partial \mathbf{D}}{\partial t} = \mathbf{J}, \quad (2.1.2)$$

$$\nabla \times \mathbf{E} + \frac{\partial \mathbf{B}}{\partial t} = 0, \quad (2.1.3)$$

$$\nabla \cdot \mathbf{B} = 0, \quad (2.1.4)$$

where  $\mathbf{E}$  and  $\mathbf{B}$  are the electric and magnetic field, respectively. The electric displacement,  $\mathbf{D}$ , and the magnetic field strength,  $\mathbf{H}$  are defined by

$$\mathbf{D} = \epsilon_0 \mathbf{E} + \mathbf{P} = \epsilon_0(1 + \chi_e) \mathbf{E} = \epsilon_0 \epsilon \mathbf{E}, \quad (2.1.5)$$

$$\mathbf{H} = \mathbf{B}/\mu_0 - \mathbf{M} = \frac{1}{\mu_0(1 + \chi_m)} \mathbf{B} = \frac{\mathbf{B}}{\mu_0 \mu}. \quad (2.1.6)$$

Here  $\epsilon_0$  and  $\mu_0$  are the vacuum permittivity and permeability,  $\epsilon$  and  $\mu$  are the permittivity and permeability of the medium.

In order to arrive at a description of a propagating wave at the interface, we take the curl of equation 2.1.3 and insert equation 2.1.2, to obtain the general wave equation:

$$\nabla \times \nabla \times \mathbf{E} = -\mu_0 \frac{\partial}{\partial t} \left( \mathbf{J} + \frac{\partial \mathbf{D}}{\partial t} \right) - \mu_0 \frac{\partial}{\partial t} (\nabla \times \mathbf{M}),$$

which for a nonmagnetic medium ( $\mathbf{M} = 0$ ) and in absence of external stimuli ( $\mathbf{J} = 0$ ), reduces to

$$\nabla \times \nabla \times \mathbf{E} = -\mu_0 \frac{\partial^2}{\partial t^2} \mathbf{D}.$$

This wave equation can be further transformed by using the following identities

$$\nabla \times \nabla \times \mathbf{E} = \nabla(\nabla \cdot \mathbf{E}) - \nabla^2 \mathbf{E}$$

and equation 2.1.1 with  $\rho = 0$

$$\nabla \cdot \mathbf{D} = \nabla \cdot (\epsilon_0 \epsilon \mathbf{E}) = \epsilon_0 (\mathbf{E} \cdot \nabla \epsilon + \epsilon \nabla \cdot \mathbf{E}) = 0.$$

From the last identity, one can deduce that  $\nabla \cdot \mathbf{E} = -\frac{1}{\epsilon_0 \epsilon} \mathbf{E} \cdot \nabla \epsilon$ . For media in which the variation in  $\epsilon$  is very small, this factor can be assumed to be zero. However, in the direction perpendicular to the interface ( $z$ -direction, see Fig.2.1),  $\epsilon$  will change abruptly

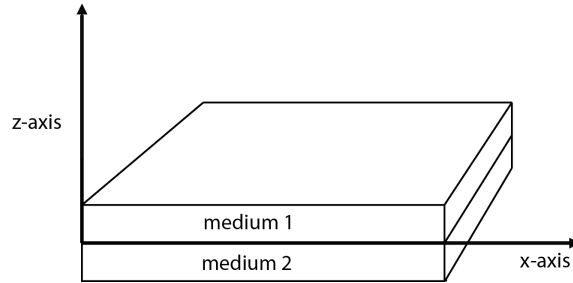


Figure 2.1: Interface ( $z = 0$ ) between two media that are characterized by the dielectric functions  $\epsilon_1$  and  $\epsilon_2$ .

when crossing the interface ( $z = 0$ ). Practically, this implies that we can make this assumption only if we are solving the wave-equation separately in both media. Therefore, neglecting spatial variation of  $\epsilon$ , the final wave equation reads

$$\nabla^2 \mathbf{E} - \frac{\epsilon}{c^2} \frac{\partial^2 \mathbf{E}}{\partial t^2} = 0.$$

Assuming harmonic time-dependence of the electric field  $\mathbf{E}$ , one obtains the so-called Helmholtz equation:

$$\nabla^2 \mathbf{E} + k_0^2 \epsilon \mathbf{E} = 0.$$

Here  $k_0$  denotes the wave vector of a propagating wave in vacuum, defined as  $k_0 = \omega/c$ . From this equation, we can derive the solution for the propagating surface wave. For this we shall use the geometry given in Fig. 2.1. It is assumed that  $\epsilon$  only changes as a function of  $z$  and that the waves propagate along the  $x$ -direction. Furthermore, we consider no spatial variation in the  $y$ -direction. Using these conditions, we can write the following relation for a plane wave propagating in the  $x$ -direction

$$\mathbf{E}(x, y, z) = \mathbf{E}(z) e^{ik_x x}, \quad (2.1.7)$$

where  $k_x$  is the component of the wave vector in the propagation direction, also referred to as the propagation constant.

An electromagnetic mode that is bound to an interface, is characterized by exponential decay with increasing distance from this interface in both half-spaces. For a single interface, such modes exist only in p-polarization (also referred to as Transverse Magnetic

polarization), i.e. polarization parallel to the interface [2]. A clear proof of this is given by Maier [1]. For the given geometry, this means that the solution we are looking for only contains  $x$ - and  $z$ -components of the electric field,

$$\mathbf{E}_j = (E_{j,x}\hat{\mathbf{x}} + E_{j,z}\hat{\mathbf{z}})e^{ik_x x - i\omega t} e^{ik_{j,z} z}, \quad j = 1, 2 \quad (2.1.8)$$

The subscript  $j$  denotes medium 1 or 2. Since the interface between the two media is 'shared', the in-plane wave vector  $k_x$  is identical for both media. Therefore, using Pythagoras, we can write the following equation for the wave vectors at the interface:

$$k_x^2 + k_{j,z}^2 = \epsilon_j k^2, \quad j = 1, 2$$

and using relation 2.1.1

$$k_x E_{j,x} + k_{j,z} E_{j,z} = 0, \quad j = 1, 2.$$

From the above two equations, one can construct an equation for a bound p-polarized wave that propagates along the interface in the  $x$ -direction

$$\mathbf{E}_j = E_{j,x}(\hat{\mathbf{x}} - k_x/k_{j,z}\hat{\mathbf{z}})e^{ik_x x - i\omega t} e^{ik_{j,z} z}, \quad j = 1, 2. \quad (2.1.9)$$

To find the solution at the interface, the equations for the electric field in both media have to be related. This can be done by applying the right boundary conditions, requiring continuity of the parallel components of  $\mathbf{E}$  and the perpendicular components of  $\mathbf{D}$  (with respect to the interface):

$$\begin{aligned} E_{1,x} - E_{2,x} &= 0, \\ \epsilon_1 E_{1,z} - \epsilon_2 E_{2,z} &= 0. \end{aligned}$$

From these equations, the frequency dependence of the wave vectors, i.e. the dispersion relations, of a mode bound to the interface can be derived:

$$k_x = \sqrt{\frac{\epsilon_1 \epsilon_2}{\epsilon_1 + \epsilon_2}} \frac{\omega}{c}, \quad (2.1.10)$$

$$k_{j,z} = \sqrt{k_x^2 - k_0^2 \epsilon_j} = \sqrt{\frac{\epsilon_j^2}{\epsilon_1 + \epsilon_2}} \frac{\omega}{c}. \quad (2.1.11)$$

Let us take a close look at these equations and study which conditions have to be fulfilled in order to obtain a propagating surface mode. For simplicity, we assume that the imaginary parts of the dielectric functions for both media are much smaller than their real parts and therefore can be neglected. Propagation in the  $x$ -direction along the interface requires that  $k_x$  has a real part. This implies that  $(\epsilon_1 \epsilon_2) \cdot (\epsilon_1 + \epsilon_2)$  has to be larger than zero. This means that the product and the sum of the dielectric functions for both media need to have the same sign. Furthermore, have exponentially decaying modes in the direction perpendicular to the interface requires  $k_{j,z}$  to be purely imaginary. This requires the sum of the dielectric functions for both media to be negative. Summing up, the conditions for a propagating bound surface mode are

$$\epsilon_1(\omega) \cdot \epsilon_2(\omega) < 0 \quad \text{and} \quad \epsilon_1(\omega) + \epsilon_2(\omega) < 0. \quad (2.1.12)$$

This implies that the dielectric function of one of the media must be negative with an absolute value larger than that of the other medium. It is well-known that noble metals have dielectric constants with a large negative real part. Therefore, bound surface modes that are propagating along the interface exist on the interfaces between a noble metals and dielectrics. However, every configuration that satisfies the above derived conditions can support these modes, f.e. heavily doped semiconductor-dielectric interfaces also support SPPs.

### 2.1.2 Properties of SPPs

As was shown above, propagating modes that are bound to the surface, are supported on interfaces between a dielectric and a conductor. The electromagnetic modes are referred to as Surface Plasmon Polaritons (SPPs). In this section we will study the dispersion relation for the in-plane wave vector, the propagation and the confinement of SPPs.

In Fig. 2.2 the in-plane wave vector of the SPP is given as a function of frequency  $\omega$ . The interface under consideration is that between a dielectric and a lossless Drude metal. For small frequencies, the penetration of the electric field into the metal is very small and therefore, the SPP behaves as light. For higher frequencies, the electric field will penetrate more and more into the metal, and the excitation will become more plasmon like. For negligible damping, the SPP wavevector goes to infinity, when the frequency approaches the surface plasmon frequency. This mode has a group velocity equal to zero and therefore,

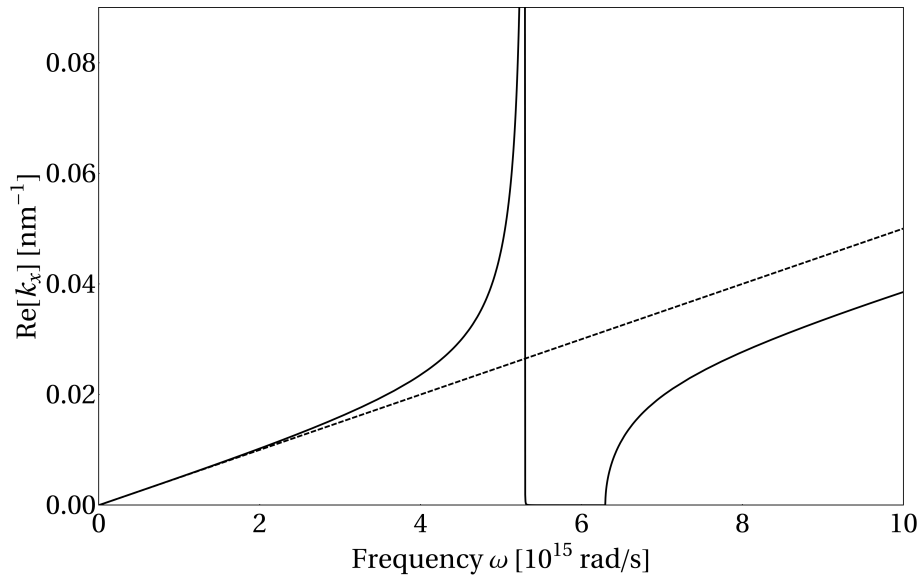


Figure 2.2: Dispersion relation for SPPs on the interface between a Drude metal with negligible damping and a glass with  $\epsilon = 2.25$  (solid line). The dashed line represents the dispersion of light in glass.

it has an electrostatic character. This mode is known as the surface plasmon [1]. Between the surface plasmon frequency  $\omega_s$  and the bulk plasma frequency  $\omega_p$ , there are no allowed modes. For frequencies higher than  $\omega_p$  the metal is transparent and bulk polariton modes will be excited. These modes are not confined to the interface and will not be studied in this project.

Comparing Fig. 2.2 with Fig. 2.3, one can see that the influence of dissipation into the metal is quite large. To take dissipation into account, the generalized Drude model for silver is used [12]

$$\epsilon(\omega) = 5.46 - 0.73 \frac{(1.72 \cdot 10^{16})^2}{\omega^2 + i\omega 8.35 \cdot 10^{13}} \quad (2.1.13)$$

When losses are present in the metal, the wavevector at the surface plasmon frequency  $\omega_s$  becomes finite. This implies that there is a lower limit on the wavelength of the surface plasmon mode and therefore, also a lower limit on the confinement to the interface (see equation 2.1.11). Another clear difference from the lossless case is that now certain modes can appear in the gap between  $\omega_s$  and  $\omega_p$ , the so-called quasi-bound modes. As can be seen from the dashed line in Fig. 2.3, the imaginary part of  $k_p$  is large in this gap and therefore, the quasi-bound modes are heavily damped and are characterized by small propagation

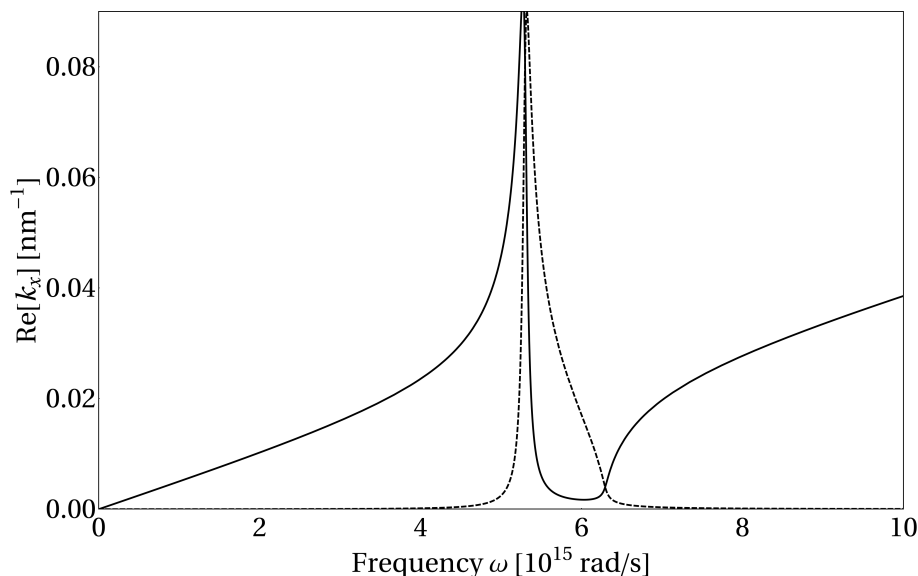


Figure 2.3: Dispersion relation for SPPs on the interface between a silver ( $\epsilon$  from equation 2.1.13) and glass with  $\epsilon = 2.25$  (solid line). Due to the presence of dissipation,  $k_\rho$  has also an imaginary part (dashed line)

lengths.

As can be seen from Fig. 2.2, the dispersion for the SPP modes lies above the light line (straight line), meaning that SPP modes have higher momenta than photons of the same frequency. This implies that SPPs cannot be excited by, e.g., a laser beam: additional momentum has to be supplied. One way to do this is by making use of phase-matching techniques, like prisms or gratings [2]. Another method to supply this extra momentum, is by applying the near field of oscillating dipoles. The near field region is the region close enough to the dipole that  $k \cdot r < 1$  is satisfied [19], where  $k$  is the wave vector of the plane waves and  $r$  is the distance to the dipole. A way to analyze this field is by looking at the equation for a plane wave  $e^{ikr}$ . Assuming that  $k$  is real,  $k = \sqrt{k_x^2 + k_y^2 + k_z^2}$  can be satisfied by a set of real  $k_x$ ,  $k_y$  and  $k_z$ . However, another possibility is a solution where f.e.  $k_y^2 + k_z^2 > k^2$ . In that case,  $k_x$  needs to be purely imaginary. For homogeneous media, these solutions are not allowed because of the solutions  $e^{|k_x|x}$  will exponentially decay for in the  $-x$ -direction, but blow up in the  $+x$ -direction, which is not allowed. However, if the homogeneity is broken by e.g. the presence of an interface, it is possible that only the exponentially decaying solution is a real solution to the system [20]. These solutions are called evanescent modes. The decay of these modes is dictated by the quantity  $kr$ . An

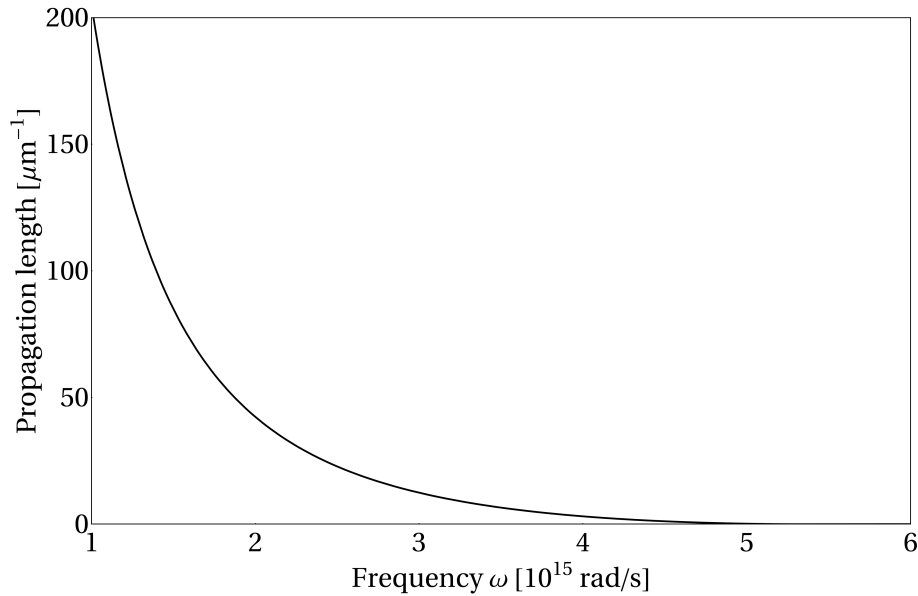


Figure 2.4: Propagation length of SPP modes on the interface between a dielectric with  $\epsilon = 2.25$  and silver ( $\epsilon$  given by equation 2.1.13)

oscillating dipole also brakes down the homogeneity in space and therefore also in this field the evanescent modes will be present. That is, in the near field of the dipole. Calculating the Poynting vector of a radiating dipole [19, ch. 6], one will find out that the near-field does not radiate. In the near field the energy transfers non-radiatively, which implies that the energy transport is not bound by the dispersion relation of light in the surrounding material. Therefore, the near field contains modes with sufficient momentum to excite SPP modes.

As was discussed earlier, to accommodate the ohmic lossless in the metal, we have to consider the dielectric function of the metal to be complex valued. From this we obtain an in-plane wave vector that has both a real and an imaginary part. The real part of this wave vector determines the wavelength of the SPP mode and the imaginary part describes the damping of the SPP propagation. A way to quantify the propagation length of the SPP mode is to look at the so-called  $1/e$  decay, i.e. the distance from the excitation point at which the exponent has become  $-1$ . The energy is proportional to the electric field modulus squared and therefore, the propagation of the surface modes (the energy attenuation length) is given by

$$L = [2k_{i,x}]^{-1}. \quad (2.1.14)$$

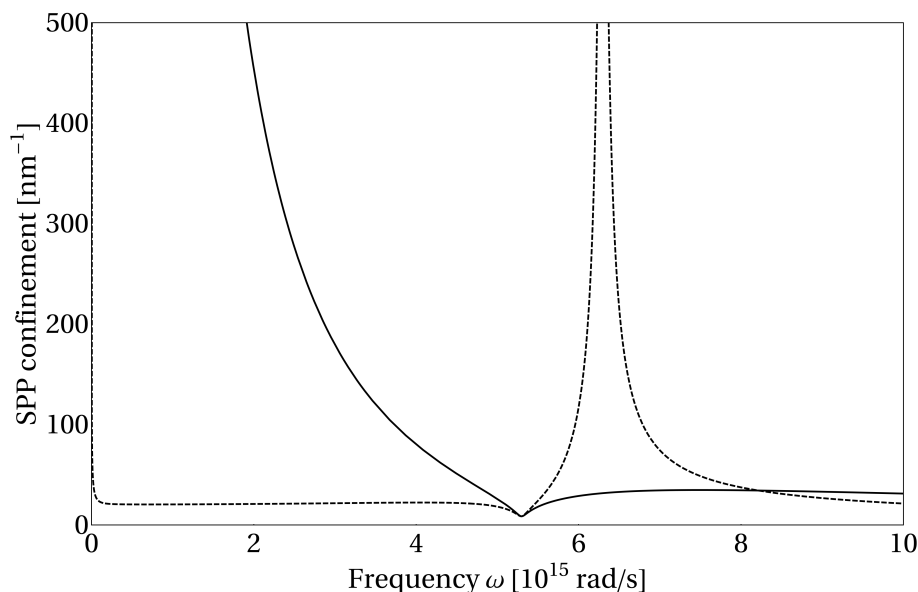


Figure 2.5: Confinement of SPP modes to the interface between a dielectric with  $\epsilon = 2.25$  and silver ( $\epsilon$  given by equation 2.1.13). The solid line gives the confinement in the dielectric. The dashed line represents the confinement in silver.

In the previous section we saw that requiring confinement to the interface, implied that the out-of-plane wave vector was purely imaginary. A common definition for the confinement to the interface is the evanescent decay length

$$\hat{z}_j = \frac{1}{|k_{j,z}|}. \quad (2.1.15)$$

Note that here the  $1/e$  decay length of the electric field is considered, rather than that of the energy. This gives a difference of a factor 2.

Figures 2.4 and 2.5 show the propagation lengths and the confinement perpendicular to the interface in the dielectric as a function of the frequency. As can be seen from these graphs, a larger propagation length corresponds to a larger extension into the dielectric (solid line) and therefore, a smaller confinement. This trade-off is typical for plasmonics. Looking closely at Fig. 2.5 several observations can be made. The figure shows that the SPP is much more confined to the interface on the side of the metal, than on the side of the dielectric. This, of course, can be explained by the fact that electric field propagate much longer in dielectrics than in metals. Another interesting point is the existence of a frequency at which the confinement in both media is minimal and, in fact, almost equal. This frequency corresponds to the surface plasmon frequency  $\omega_s$ . Furthermore, it



is interesting to note that there is a maximum in confinement to the silver. The frequency at which this maximum occurs, is the plasmon frequency of the silver. At this frequency, the skin depth of the silver for the electric field becomes quite large and the field can extend more into the metal. As discussed earlier, for frequency higher than  $\omega_s$  the modes are not propagating bound surface modes anymore, and therefore we will not go into further detail on these modes. The SPP propagation length for the given interface ranges from around  $35 \mu\text{m}$  to  $5 \mu\text{m}$  in the visible regime. The confinement in the dielectric is between  $300 \text{ nm}$  to  $50 \text{ nm}$  and the confinement in the silver is more or less constant at  $25 \text{ nm}$ .

## 2.2 Response of a Metal Nanosphere to an Oscillating Electric Field

As was discussed in the previous section, one way to excite surface plasmon polaritons is by making use of the near field of an oscillating dipole. In this section it will be shown that the response of a metal nanoparticle to an oscillating electric field can be modeled as the response of a driven dipolar oscillator.

For calculating the scattering and absorption of an electric field by a sphere, the exact theory derived by Gustav Mie in 1908 [3], can be used. However, this theory is mathematically very elaborate and therefore, it is difficult to understand the important physical processes.

Since in this project we are considering the guiding of light at sub-wavelength scale, we can use the so-called quasi-static approximation. The condition for this simplification is that the particle size is much smaller than the wavelength of the applied field in the surrounding medium. This implies that the spatial phase of the oscillating field is practically constant over the particle volume. Under this condition, the problem is reduced to the problem of a particle in an electrostatic field (for more details, see [1] and [4]). This approximation is called quasi-static, because the magnitude and direction of dipole moment induced in the sphere are calculated in the static case, whereas it assumes that this dipole moment oscillates with the same frequency as the applied field under dynamic conditions.

The problem of a sphere in an electrostatic field is very clearly discussed in [19, sec. 4.4] and only the final result will be reproduced here. The dipole moment of sphere, with

permittivity  $\epsilon$  and radius  $a$ , embedded in host medium with permittivity  $\epsilon_m$ , in a static electric field with amplitude  $E_0$ , is given by

$$\mathbf{p} = 4\pi\epsilon_0\epsilon_m a^3 \frac{\epsilon(\omega) - \epsilon_m}{\epsilon(\omega) + 2\epsilon_m} \mathbf{E}_0. \quad (2.2.1)$$

Thus, the applied electric field  $\mathbf{E}_0$  induces a dipole with the same direction as  $\mathbf{E}_0$ , and a magnitude depending on the permittivities of the media, the radius of the sphere and the amplitude of the applied field. At this point, it is convenient to introduce the sphere polarizability  $\alpha$ , which determines how the induced dipole moment is related to the applied field,  $\mathbf{p} = \epsilon_0\epsilon_m\alpha\mathbf{E}_0$ , where

$$\alpha = 4\pi a^3 \frac{\epsilon(\omega) - \epsilon_m}{\epsilon(\omega) + 2\epsilon_m}. \quad (2.2.2)$$

In general the permittivities of the sphere and the host medium are frequency dependent. However, when considering a metal nanosphere embedded in a dielectric surrounding, it is usually assumed that only the metal sphere permittivity  $\epsilon$  is frequency dependent. The frequency dependence of  $\epsilon$  gives rise to a resonance in the polarizability. This resonance will occur at the frequency for which the denominator of equation 2.2.2 reaches a minimum. Assuming that the imaginary part of  $\epsilon$  varies much slower with the frequency than the real part, the resonance condition is

$$Re[\epsilon(\omega)] = -2\epsilon_m \quad (2.2.3)$$

This relation is referred to as the Fröhlich condition, and the associated mode is the dipole surface plasmon [1].

Some care has to be taken when using this model, because the discrepancy with the result from the exact Mie theory can be quite large. A way to overcome this, is to add the following correction factors. These can be derived by including the depolarization field, a field generated by the polarized matter of the sphere that is opposing the external field [18]:

$$\frac{1}{\alpha} = \frac{1}{\alpha^{(0)}} - \frac{k^2}{a} - \frac{2i}{3}k^3. \quad (2.2.4)$$

Here,  $\alpha^{(0)}$  is the polarizability that was defined earlier in equation 2.2.2. This term is referred to as the bare polarizability, because there are no correction factor present. The  $k^2$  term describes the depolarization shift, a redshift of the plasmon resonance due to the

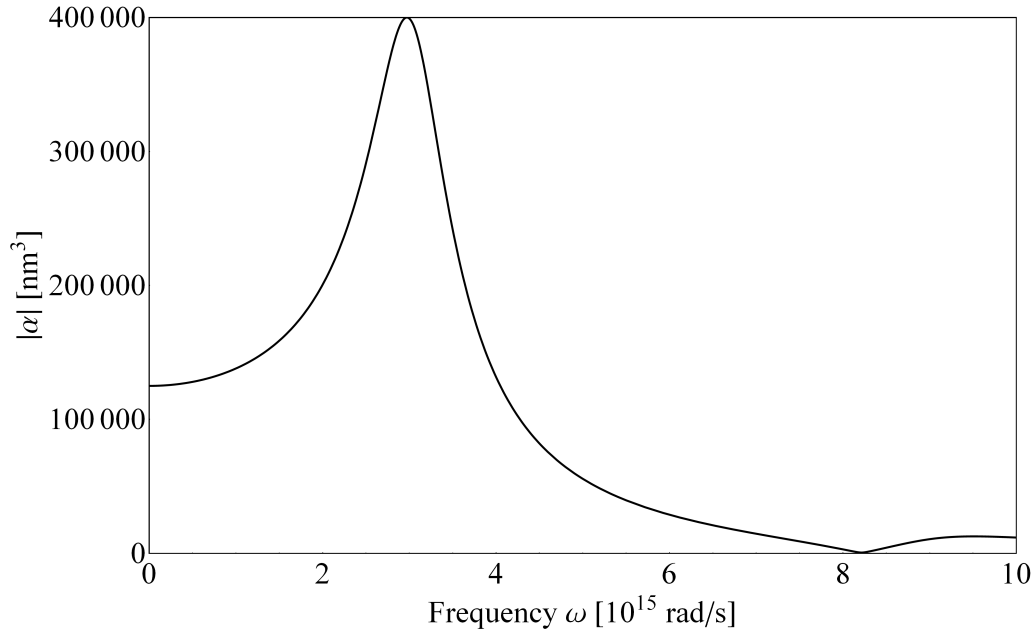


Figure 2.6: The absolute value of the polarizability  $\alpha$  (from equation 2.2.4) for a silver sphere of  $a = 50 \text{ nm}$  embedded in a dielectric with  $\epsilon_m = 2.25$ . The permittivity of the metal is given by the generalized Drude model from equation 2.1.13.

presence of the depolarization field. The  $k^3$  term describes the radiative losses and are important for energy conservation (see [12] and references therein). It should be noted that although the resonance condition for the surface plasmon mode will change when these corrections are included, the resonance will still occur. The importance of the result represented in equation 2.2.4 is that it implies that the size of the sphere only enters in determining the magnitude of the dipole moment, but the physical volume of the sphere can be ignored. This means that for spheres that are much smaller than the wavelength of the exciting field, the sphere can be modeled as an ideal, point-like dipole.

## 2.3 An oscillating dipole close to an interface

### 2.3.1 Deriving the equations for the electric field

Using the fact that a metal nanoparticle can be treated as an oscillating point dipole, we shall now derive the electric field of the dipole above an arbitrary medium. For this we will follow the method developed by Arnold Sommerfeld for the calculation of the field

produced by a radio antenna close to the earth [14], [21].

According to Hertz [22], we can write for the fundamental potential for a dipole oscillating in free space as

$$\mathbf{\Pi} = \frac{\mathbf{i}}{R} e^{i(kR - \omega t)}, \quad (2.3.1)$$

where  $R$  is the distance between the source and the point of calculation,  $k$  is the wave vector corresponding to the oscillating field,  $\omega$  is the frequency of the oscillating dipole, and  $t$  denotes the time. The time-dependence will be ignored in the rest of this text.  $\mathbf{\Pi}$  is the Hertz vector potential and, for a dipole oscillating in a homogeneous environment, has the direction of the oscillation of the dipole. From this vector potential, we can calculate  $\mathbf{E}$  and  $\mathbf{H}$  by

$$\mathbf{E} = k^2 \mathbf{\Pi} + \nabla(\nabla \cdot \mathbf{\Pi}), \quad \mathbf{H} = \frac{k^2}{\mu_0 i \omega} \nabla \times \mathbf{\Pi} \quad (2.3.2)$$

In order to calculate the electric field produced by an oscillating dipole close to an interface, we have to find the Hertz vector potential for this geometry. The most important step in Sommerfeld's method is to rewrite the spherical waves of 2.3.1 as a superposition of plane waves. The reason for doing this that, from the work of Fresnel, the solution for plane waves reflection on an interface is known.

Expressing the vector potential of an isolated dipole as a superposition of plane waves can be done by using the following identity

$$\Pi = \int_0^\infty F(k_\rho) J_0(k_\rho \rho) e^{\pm i k_z z} dk_\rho, \quad (2.3.3)$$

which is referred to as the 'Sommerfeld'-identity. The vector character is omitted here, because the dipole can be oriented in an arbitrary direction. In this equation,  $\rho$  and  $z$  are the coordinates in the parallel direction and the perpendicular direction with respect to the interface (cylindrical coordinates). The wave vectors  $k_\rho$  and  $k_z$  are the wave vector components in the radial and perpendicular direction, respectively. The function  $J_0$  is the standard (cylindrical) Bessel function of zeroth order. The physical interpretation of the Sommerfeld-identity is that a spherical wave can be rewritten as a superposition of the product of cylindrical waves, propagating parallel to the interface, and plane waves, propagating perpendicular to the interface. The function  $F(k_\rho)$  is a function that has to

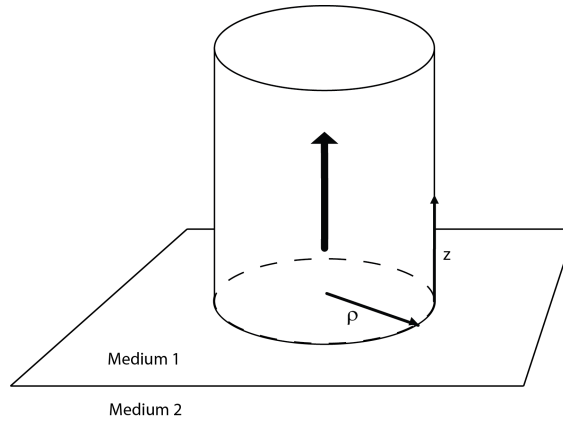


Figure 2.7: The coordinate system for using the Sommerfeld identity

be determined in order to match equation 2.3.4 with  $e^{ikR}/R$  exactly. A clear calculation of this factor is presented in [14]. The final result reads

$$\Pi = \frac{e^{ikR}}{R} = \int_0^\infty J_0(k_\rho \rho) e^{ik_z |z|} \frac{k_\rho dk_\rho}{-ik_z}, \quad (2.3.4)$$

where  $R$  is again the distance between the dipole source and the point of calculation and, in terms of  $\rho$  and  $z$ , is given by

$$R = \sqrt{\rho^2 + z^2}.$$

In order to satisfy the radiation conditions, namely the field goes to zero if the distance from the source goes to infinity,  $k_z$  has to be taken with the positive imaginary part

$$k_z = \sqrt{k^2 - k_\rho^2}, \quad \text{Im}[k_z] \geq 0.$$

### Dipole oscillating perpendicular to the interface

Let us consider a geometry given in Fig. 2.8. The oscillating dipole is embedded in medium 1 at a height  $z = h$  above the interface. At an arbitrary point in medium 1, the field will acquire two contributions: the (direct) field that comes directly from the dipole and the (indirect) field that is reflected from the interface. This reflected field can actually be thought of as the field coming from an image dipole induced in medium 2. At an arbitrary point in medium two, only the part of the field that is transmitted through the interface can be measured. In this system, it is convenient to define the Hertz vector potential  $\mathbf{\Pi}$  in the  $z$ -direction, because we are considering a dipole oscillating in  $z$ -direction. This

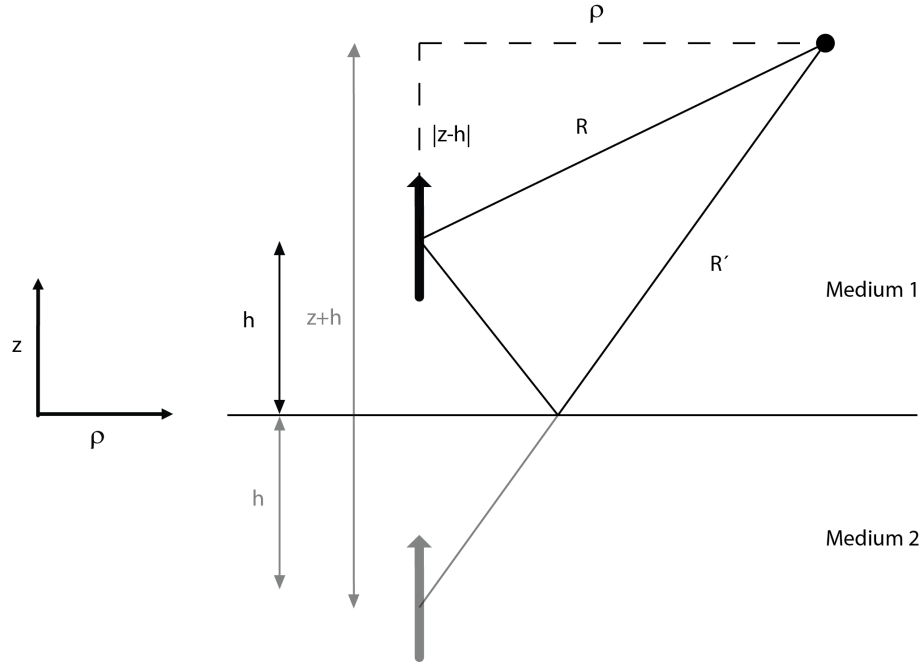


Figure 2.8: The geometry under consideration for the deriving the vector potential of a dipole oscillating perpendicular to the interface.

implies that this vector will only have a  $z$ -component. Therefore, throughout the following derivation,  $\mathbf{\Pi}$  will be written as  $\Pi$ .

Using equation 2.3.4 and looking at the given geometry, we can write down the following potentials for the dipoles in medium 1 and medium 2

$$\begin{aligned} \Pi_1 &= \Pi_{1,direct} + \Pi_{1,indirect} \\ &= \int_0^\infty J_0(k_\rho \rho) e^{ik_{1,z}|z-h|} \frac{k_\rho dk_\rho}{-ik_{1,z}} + \int_0^\infty F_1(k_\rho) J_0(k_\rho \rho) e^{ik_{1,z}(z+h)} dk_\rho, \end{aligned} \quad (2.3.5)$$

$$\Pi_2 = \Pi_{2,indirect} = \int_0^\infty F_2(k_\rho) J_0(k_\rho \rho) e^{-ik_{2,z}z + ik_{1,z}h} dk_\rho. \quad (2.3.6)$$

The subscripts 1 and 2 refer to medium 1 and 2, respectively. The functions  $F_1$  and  $F_2$  can be determined from the boundary conditions at the interface ( $z = 0$ ). In the equation for  $\Pi_2$ , the factor  $\exp[ik_{1,z}h]$  is added for convenience, which is allowed because this will only change the function  $F_2(k_\rho)$ , still to be determined. From Maxwell's equations we know that for the dipole oscillating perpendicular to the interface, the continuity of the tangential components of  $\mathbf{E}$  and  $\mathbf{H}$  is required, i.e.  $E_\rho$  and  $H_\phi$ . According to equations 2.3.2 this gives

$$E_\rho = \frac{\partial}{\partial \rho} \frac{\partial \Pi_1}{\partial z}, \quad H_\phi = \frac{-k_1^2}{\mu_0 i \omega} \frac{\partial \Pi_1}{\partial \rho} \quad \text{in medium 1,}$$

$$E_\rho = \frac{\partial}{\partial \rho} \frac{\partial \Pi_2}{\partial z}, \quad H_\phi = \frac{-k_2^2}{\mu_0 i \omega} \frac{\partial \Pi_2}{\partial \rho} \quad \text{in medium 2.}$$

Therefore, the following relations should hold at the interface

$$\frac{\partial}{\partial \rho} \frac{\partial \Pi_1}{\partial z} = \frac{\partial}{\partial \rho} \frac{\partial \Pi_2}{\partial z} \quad \text{and} \quad k_1^2 \frac{\partial \Pi_1}{\partial \rho} = k_2^2 \frac{\partial \Pi_2}{\partial \rho}$$

Since all of these equations contain a partial derivative to  $\rho$ , we can integrate them with respect to  $\rho$  and end up with:

$$\frac{\partial \Pi_1}{\partial z} = \frac{\partial \Pi_2}{\partial z} \quad \text{and} \quad \epsilon_1 \Pi_1 = \epsilon_2 \Pi_2, \quad (2.3.7)$$

where we used that the fields have to vanish for large  $\rho$  and that  $k_1^2/k_2^2 = \epsilon_1/\epsilon_2$ . According to these conditions, two equations have to be solved, namely

$$k_\rho + ik_{1,z}F_1 + ik_{2,z}F_2 = 0$$

and

$$\epsilon_2 F_2 = \epsilon_1 \left( i \frac{k_\rho}{k_{1,z}} + F_1 \right).$$

Inserting the results in equations 2.3.5 and 2.3.6 yields

$$\begin{aligned} \Pi_1 = & \int_0^\infty J_0(k_\rho \rho) e^{ik_{1,z}|z-h|} \frac{k_\rho dk_\rho}{-ik_{1,z}} + \int_0^\infty J_0(k_\rho \rho) e^{ik_{1,z}(z+h)} \frac{k_\rho}{-ik_{1,z}} dk_\rho \\ & - 2i \int_0^\infty J_0(k_\rho \rho) \frac{k_\rho}{k_{1,z}} \frac{\epsilon_1 k_{2,z}}{\epsilon_1 k_{2,z} + \epsilon_2 k_{1,z}} e^{ik_{1,z}(z+h)} dk_\rho. \end{aligned}$$

Again using the Sommerfeld-identity from equation 2.3.4 this can be rewritten as

$$\Pi_1 = \frac{e^{ikR}}{R} + \frac{e^{ikR'}}{R'} - 2i \int_0^\infty J_0(k_\rho \rho) \frac{k_\rho}{k_{1,z}} \frac{\epsilon_1 k_{2,z}}{\epsilon_1 k_{2,z} + \epsilon_2 k_{1,z}} e^{ik_{1,z}(z+h)} dk_\rho, \quad (2.3.8)$$

and similar for the potential in medium 2,

$$\Pi_2 = -2i \int_0^\infty J_0(k_\rho \rho) \frac{\epsilon_1 k_\rho}{\epsilon_1 k_{2,z} + \epsilon_2 k_{1,z}} e^{-ik_{2,z}z + ik_{1,z}h} dk_\rho. \quad (2.3.9)$$

Here,  $k_\rho$  is the wave vector in the radial direction,  $k_{j,z}$  is the wave vector perpendicular to the interface in medium  $j$ ,  $h$  is the distance between the dipole and the interface.  $R = \sqrt{\rho^2 + (z - h)^2}$  and  $R' = \sqrt{\rho^2 + (z + h)^2}$  are the distances from the dipole and its image, with respect to the point of calculation.

### Dipole oscillating parallel to the interface

For calculating the field of a dipole oscillating parallel to the interface, one needs to set the Hertz vector to  $\mathbf{\Pi} = (\Pi_x, 0, \Pi_z)$ , instead of just in the direction of the oscillation. The reason for this is that in the reflected field, both  $s$ - and  $p$ -polarized modes will be present (for more details, see [21, p.257]).

We will first derive the  $x$ -component of the potential, following the same procedure as in the previous section. From the continuity of the  $x$ - and  $y$ -components of  $\mathbf{E}$  on the interface, we can write

$$\nabla \cdot \mathbf{\Pi}_1 = \nabla \cdot \mathbf{\Pi}_2 \quad \text{and} \quad k_1^2 \Pi_{1,x} = k_2^2 \Pi_{2,x}$$

which leads to

$$\epsilon_1 \Pi_{1,x} = \epsilon_2 \Pi_{2,x} \quad \text{and} \quad \epsilon_1 \frac{\partial \Pi_{1,x}}{\partial z} = \epsilon_2 \frac{\partial \Pi_{2,x}}{\partial z}.$$

Applying these equations to the potentials given in equations 2.3.5 and 2.3.6 and solving for  $F_1$  and  $F_2$ , we arrive at

$$\Pi_{1,x} = \frac{e^{ikR}}{R} - \frac{e^{ikR'}}{R'} + 2i \int_0^\infty J_0(k_\rho \rho) \frac{k_\rho}{k_{1,z} + k_{2,z}} e^{ik_{1,z}(z+h)} dk_\rho, \quad (2.3.10)$$

and for  $\Pi_{2,x}$

$$\Pi_{2,x} = 2i \frac{\epsilon_1}{\epsilon_2} \int_0^\infty J_0(k_\rho \rho) \frac{k_\rho}{k_{1,z} + k_{2,z}} e^{-ik_{2,z}z + ik_{1,z}h} dk_\rho. \quad (2.3.11)$$

For the  $z$ -component of the Hertz potential, the boundary conditions can be determined from the continuity of  $H_x$  and  $H_y$

$$H_{1,x} = \frac{k_1^2}{i\mu_0\omega} \frac{\partial \Pi_{1,z}}{\partial y}, \quad H_{1,y} = \frac{k_1^2}{i\mu_0\omega} \left( \frac{\partial \Pi_{1,x}}{\partial z} - \frac{\partial \Pi_{1,z}}{\partial x} \right) \quad \text{in medium 1}$$

$$H_{2,x} = \frac{k_2^2}{i\mu_0\omega} \frac{\partial \Pi_{2,z}}{\partial y}, \quad H_{2,y} = \frac{k_2^2}{i\mu_0\omega} \left( \frac{\partial \Pi_{2,x}}{\partial z} - \frac{\partial \Pi_{2,z}}{\partial x} \right) \quad \text{in medium 2}$$



Equating the expressions for  $H_x$  and  $H_y$  for  $z = 0$  we obtain

$$\epsilon_1 \Pi_{1,z} = \epsilon_2 \Pi_{1,z}, \quad \text{and} \quad \frac{\partial \Pi_{1,z}}{\partial z} - \frac{\partial \Pi_{2,z}}{\partial z} = \frac{\partial \Pi_{1,x}}{\partial x} - \frac{\partial \Pi_{2,x}}{\partial x} \quad (2.3.12)$$

As can be seen from the above equations, the derivative of the  $x$ -component of the potential with respect to the  $x$  coordinate has to be calculated. Since  $\Pi_x$  depends on  $\rho = \sqrt{x^2 + y^2}$ , a  $\cos \phi$  factor will enter the equation, where  $\phi$  is the angle between  $x$  and  $r$ . This implies that the previously used cylindrical eigenfunctions in the Sommerfeld-identity,  $J_0(k_\rho \rho) e^{ik_z z}$ , can not be used to construct  $\Pi_z$ . Rather, the cylindrical eigenfunctions with the next higher index have to be used (see [21, p.177]), that is  $J_1(k_\rho \rho) e^{k_z z} \cos \phi$ . Using these eigenfunctions, the equations for  $\Pi_z$  become

$$\begin{aligned} \Pi_{1,z} &= \cos \phi \int_0^\infty J_1(k_\rho \rho) \Phi_1(k_\rho) e^{ik_{1,z}(z+h)} dk_\rho \\ \Pi_{2,z} &= \cos \phi \int_0^\infty J_1(k_\rho \rho) \Phi_2(k_\rho) e^{-ik_{2,z}z + ik_{1,z}h} dk_\rho. \end{aligned}$$

Applying the boundary conditions 2.3.12 and solving for  $\Phi_1$  and  $\Phi_2$ , finally gives

$$\Pi_{1,z} = -\frac{2}{k_1^2} \cos \phi \int_0^\infty J_1(k_\rho \rho) k_\rho^2 \frac{\epsilon_1(k_{1,z} - k_{2,z})}{\epsilon_1 k_{2,z} + \epsilon_2 k_{1,z}} e^{ik_{1,z}(z+h)} dk_\rho, \quad (2.3.13)$$

$$\Pi_{2,z} = -\frac{2}{k_2^2} \cos \phi \int_0^\infty J_1(k_\rho \rho) k_\rho^2 \frac{\epsilon_1(k_{1,z} - k_{2,z})}{\epsilon_1 k_{2,z} + \epsilon_2 k_{1,z}} e^{-ik_{2,z}z + ik_{1,z}h} dk_\rho. \quad (2.3.14)$$

### Calculating the Electric Field

To sum up, the results of the derivation of the Hertz vector potential will be given for an oscillating dipole embedded in medium 1 (characterized by  $\epsilon_1$ ), at a height  $h$  above medium 2 (characterized by  $\epsilon_2$ ), and the corresponding electric field will be calculated.

The potentials in medium 1 for a dipole oscillating perpendicular (in  $z$ -direction) and parallel (in  $x$ -direction) to interface, are given by

$$\mathbf{\Pi}_{1,\perp} = \begin{pmatrix} 0 \\ 0 \\ \frac{e^{ikR}}{R} + \frac{e^{ikR'}}{R'} - 2i \int_0^\infty J_0(k_\rho \rho) \frac{k_\rho}{k_{1,z}} \frac{\epsilon_1 k_{2,z}}{\epsilon_1 k_{2,z} + \epsilon_2 k_{1,z}} e^{ik_{1,z}(z+h)} dk_\rho \end{pmatrix} \quad (2.3.15)$$

$$\mathbf{\Pi}_{1,\parallel} = \begin{pmatrix} \frac{e^{ikR}}{R} - \frac{e^{ikR'}}{R'} + 2i \int_0^\infty J_0(k\rho\rho) \frac{k_\rho}{k_{1,z}+k_{2,z}} e^{ik_{1,z}(z+h)} dk_\rho \\ 0 \\ -\frac{2}{k_1^2} \cos \phi \int_0^\infty J_1(k\rho\rho) \frac{\epsilon_1(k_{1,z}-k_{2,z})}{\epsilon_1 k_{2,z} + \epsilon_2 k_{1,z}} k_\rho^2 e^{ik_{1,z}(z+h)} dk_\rho \end{pmatrix} \quad (2.3.16)$$

The potentials in medium 2, created by a dipole oscillating in medium 1 are

$$\mathbf{\Pi}_{2,\perp} = \begin{pmatrix} 0 \\ 0 \\ 2i \int_0^\infty J_0(k\rho\rho) \frac{k_\rho}{k_{1,z}} \frac{\epsilon_1 k_\rho}{\epsilon_1 k_{2,z} + \epsilon_2 k_{1,z}} e^{-ik_{2,z}z + ik_{1,z}h} dk_\rho \end{pmatrix} \quad (2.3.17)$$

$$\mathbf{\Pi}_{2,\parallel} = \begin{pmatrix} 2i \frac{\epsilon_1}{\epsilon_2} \int_0^\infty J_0(k\rho\rho) \frac{k_\rho}{k_{1,z}+k_{2,z}} e^{-ik_{2,z}z + ik_{1,z}h} dk_\rho \\ 0 \\ -\frac{2}{k_2^2} \cos \phi \int_0^\infty J_1(k\rho\rho) k_\rho^2 \frac{\epsilon_1(k_{1,z}-k_{2,z})}{\epsilon_1 k_{2,z} + \epsilon_2 k_{1,z}} e^{-ik_{2,z}z + ik_{1,z}h} dk_\rho \end{pmatrix} \quad (2.3.18)$$

Note that in this derivation, the  $x$ -component is chosen as the parallel component. Of course, the exact same procedure can be followed for the  $y$ -direction, because the cylindrical symmetry. From these Hertz vector potentials, the electric field in medium  $j$  can be calculated using the following relation

$$\mathbf{E} = \frac{1}{\epsilon_j} [k_j^2 \mathbf{\Pi}_j + \nabla(\nabla \cdot \mathbf{\Pi}_j)], \quad j = 1, 2. \quad (2.3.19)$$

For calculating the electric field in medium 1, produced by a dipole oscillating in medium 1 and perpendicular to the interface, i.e.  $\mathbf{\Pi} = \Pi_z \hat{\mathbf{z}}$ , this will become

$$\mathbf{E}_\perp = \frac{1}{\epsilon_1} \begin{pmatrix} \frac{\partial}{\partial x} \frac{\partial}{\partial z} \Pi_z \\ \frac{\partial}{\partial y} \frac{\partial}{\partial z} \Pi_z \\ k_1^2 \Pi_z + \frac{\partial^2}{\partial z^2} \Pi_z \end{pmatrix}. \quad (2.3.20)$$

As an example, the equation for the  $z$ -component of the electric field produced by a dipole oscillating in the  $z$ -direction, is shown below (the equations for the other components can be found in the appendix):

$$\begin{aligned} \vec{E}_{z,z} = & \frac{1}{\epsilon_1} \left[ \left( k_1^2 + \frac{(3 - 3ik_1R - k_1^2R^2)(z-h)^2 + ik_1R^3 - R^2}{R^4} \right) \frac{e^{ik_1R}}{R} \right. \\ & + \left( k_1^2 + \frac{(3 - 3ik_1R' - k_1^2R'^2)(z+h)^2 + ik_1R'^3 - R'^2}{R'^4} \right) \frac{e^{ik_1R'}}{R'} \\ & \left. - 2i \int_0^\infty J_0(k\rho\rho) \frac{k_\rho^3}{k_{1,z}} \frac{\epsilon_1 k_{2,z}}{\epsilon_1 k_{2,z} + \epsilon_2 k_{1,z}} e^{ik_{1,z}(z+h)} dk_\rho \right]. \end{aligned} \quad (2.3.21)$$

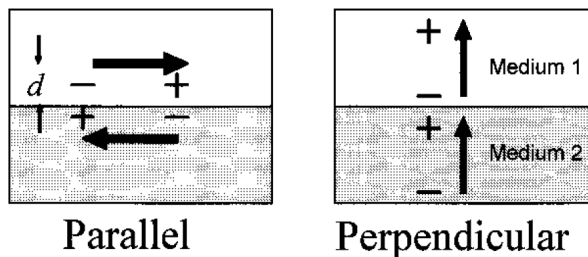


Figure 2.9: The effect of the image dipole on the total dipole strength for a dipole close to a reflecting interface. Figure reproduced from [25]

Taking a close look at this equation, one can recognize several different contributions. The first term can be identified as the field produced by an oscillating dipole in a homogeneous environment (without an interface). Comparing the first term to the second, one notices that this field is also corresponding to a homogeneous environment, but the location of the dipole is different. This dipole is the mirror image of the source dipole, induced in medium 2. Physically, this corresponds to the field that is reflected from a perfectly reflecting interface. This can be checked by setting medium 2 as a perfect reflector, i.e.  $\epsilon_2 \rightarrow \infty$ . The integral contribution will vanish and the total field is given by the sum of the first two terms. Comparing the potentials in equations A.2.1 and A.2.2, one should notice that for a dipole oscillating parallel to the surface the image dipole has the opposite sign. This can be easily understood by looking at Fig. 2.9.

The last term is a so-called Sommerfeld-integral and can be thought of as a correction factor for how much the interface deviates from being a perfect reflector. Physically, it refers to surface currents that are induced at the interface. It is important to note that (for p-polarized modes) there is a singularity for  $\epsilon_1 k_{2,z} + \epsilon_2 k_{1,z} = 0$ . Calculating the in-plane wave vector  $k_p = p$  that satisfies this equality, gives

$$p = \sqrt{\frac{\epsilon_1 \epsilon_2}{\epsilon_1 + \epsilon_2} \frac{\omega}{c}}, \quad (2.3.22)$$

which corresponds exactly to the in-plane wave vector of a bound surface mode, as was derived from Maxwell's equations in section 2.1.

Another point worth noting is that the Sommerfeld integral in the Hertz vector potential for a dipole oscillating perpendicular to the interface describe p-polarized modes. For a dipole oscillating parallel to the interface there are two nonzero components of the Hertz vector. The component perpendicular to the interface again contains an integral describ-

ing p-polarized modes. However, the integral in the component parallel to the interface describes s-polarized modes. As was mentioned in section 2.1 (a proof is given in [1]), SPP-modes can only exist in p-polarization. This implies that for a dipole oscillating perpendicular to the interface the excited surface modes are only p-polarized, whereas for a horizontal dipole both s- and p-polarized modes will be excited. This means that dipoles oscillating perpendicular to the interface can couple to SPP-modes more efficiently.

This integral needs to be evaluated numerically, but due to the mathematically awkward behavior of the integrand, a special evaluation method is needed. A recipe for the calculation of the Sommerfeld-integrals will be given in section 2.3.3.

### 2.3.2 Coupling to SPP modes

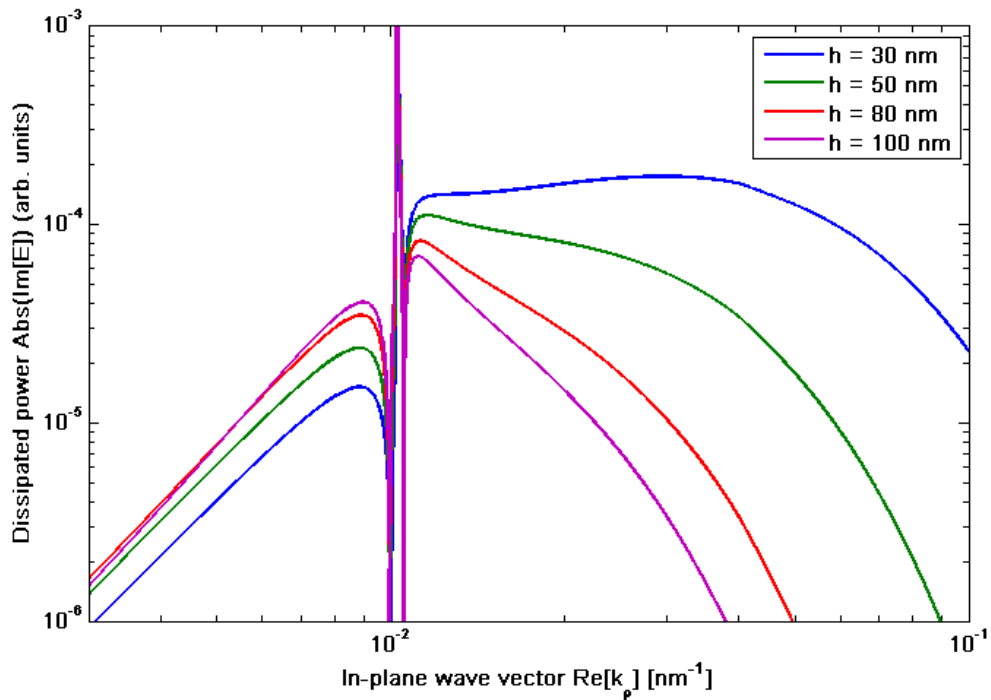


Figure 2.10: The imaginary part of the integrand of equation 2.3.23 as a function of the in-plane wavevector  $k_\rho$  for different dipole-interface separations  $h$ . The peak at  $k_\rho \approx 10^{-2}$  corresponds to the singularity at  $k_{rh_0} = k_1$ . The peak to the right of this is due to the singularity giving the SPP mode. The dipole (in vacuum) is oscillating perpendicular to the interface of a silver half-space. The excitation wavelength is 600 nm and for the permittivity of the silver the generalized drude model is used.

As the electric field of a dipole close to an interface is known, the influence of the interface on the dipole can be studied. Specifically, we would like to know the change in radiation and decay properties due to the presence of the surface and study the influence of SPPs as a decay channel. To do this, we will use the method proposed by Chance, Prock and Silbey in their paper about molecular fluorescence near interfaces [24] and a review paper by Barnes, where he discussed the influence of the photonic mode density on fluorescence [25]. In order not to confuse notation, we will not separate the scattered field into that of the image dipole and the surface currents, but combine the last two terms of equation 2.3.8 to one integral. Calculating the electric field from this potential at the dipole position and omitting the direct contribution to the field, we obtain

$$E_z(\rho = 0, z = h) = -\frac{1}{\epsilon_1} \int_0^\infty \left( \frac{\epsilon_1 k_{2,z} - \epsilon_2 k_{1,z}}{\epsilon_1 k_{2,z} + \epsilon_2 k_{1,z}} \right) \frac{k_\rho^3}{-ik_{1,z}} e^{2ik_{1,z}h} dk_\rho \quad (2.3.23)$$

The damping rate of the oscillating dipole is dictated by the imaginary part of the reflected field at the dipole position [24]. Therefore, by plotting the imaginary part of the integrand above, we can see how the energy dissipation is related to the in-plane wave vector  $k_\rho$ . This plot is given in Fig. 2.10. Wavevectors smaller than  $k_1$  correspond to radiative decay, while the larger wavevectors refer to non-radiative decay. In this figure the coupling to the SPP modes is clearly visible and it is a major decay channel (nb. the logarithmic scale). Also, it becomes clear from this figure that for smaller separations between the dipole and the interface the coupling higher wave vector modes becomes more important and is competing with the SPP decay channel. People refer to these modes as 'lossy surface waves', since they are not propagating on the interface, but decaying exponentially into both media.

### 2.3.3 Calculating the Sommerfeld-integrals

Sommerfeld-integrals are general type of integrals, that will come into play when a dipole close to a non-perfect reflector is considered. Since the first publication on this topic by Arnold Sommerfeld in 1909 [14], much research has been done on the best and most efficient methods to evaluate these integrals.

In this section, two different calculation methods will be presented. The first method is the one proposed by Sommerfeld himself. The second is a method that was published by Paulus et al [23].

Let us first look at the integrand in equation 2.3.21 more closely. The reason why this integral does not allow straightforward evaluation, is because of the presence of branch cuts and singularities. The branch cuts are present due to the double-valued complex square-roots

$$k_{1,z} = \sqrt{k_1^2 - k_\rho^2} \quad \text{and} \quad k_{2,z} = \sqrt{k_2^2 - k_\rho^2},$$

which make the complex plane consist of 4 Riemann sheets, each corresponding to a different combination of the + and - signs of the above square-roots. Furthermore, the integrand has singularities at  $k_{1,z} = 0$  and at  $\epsilon_1 k_{2,z} + \epsilon_2 k_{1,z} = 0$ . The latter deserves special attention, because the in-plane wavevector  $k_\rho = p$  for which this equality is satisfied, corresponds exactly to the wave vector of the bound surface modes (see equation 2.3.22). This means that when one considers an interface between a dielectric ( $\epsilon_1 > 0$ ) and a metal ( $\epsilon_2 < 0$ ), the singularity corresponds exactly to the SPP wave vector.

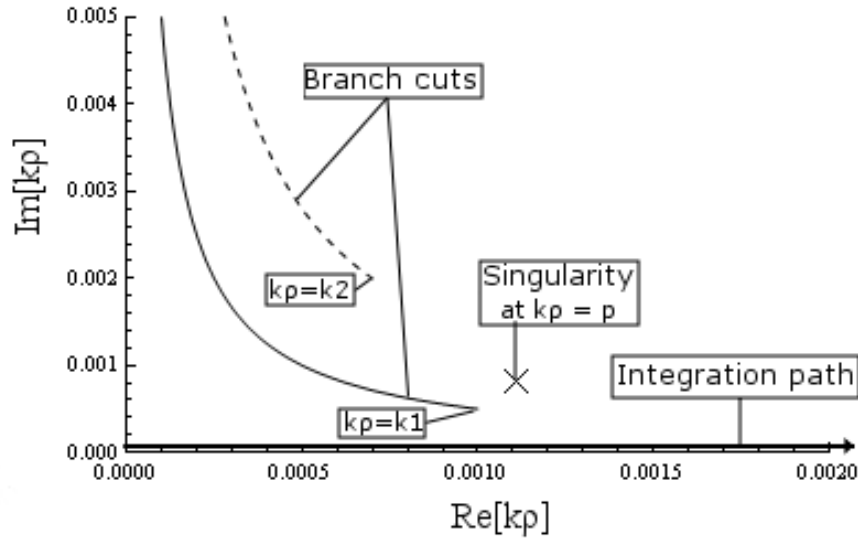


Figure 2.11: Plane of integration for the Sommerfeld integral from equation 2.3.21. The branch cuts due to the double valued functions  $k_{1,z}$  and  $k_{2,z}$  are indicated by the solid and dashed lines, respectively. The cross indicates the singularity. The integration path runs along the real axis.

An overview of these features of the integrand in equation 2.3.21 is given in Fig. 2.11. The branch cuts of a multivalued function may be chosen arbitrarily. For reasons that will become clear later, we decided to cut the complex plane at the lines on which the

imaginary parts of  $k_{1,z}$  and  $k_{2,z}$  are zero. The integration path drawn in Fig. 2.11 runs along the real axis.

To study excitation and guiding of SPPs, we need to calculate the integral for a dielectric-metal interface. We define medium 1 as a dielectric and medium 2 as a metal. In general, the dissipation of light in a dielectric is very low, which implies that  $k_1$  will have a very small imaginary part and will therefore lie close to the integration path. Also, the singularity corresponding to the SPP mode will come closer to this path for a dielectric with smaller losses. The presence of these features close to the real axes, makes integration along the real axis numerically unstable and a different path has to be used.

### Integration along the branch cuts

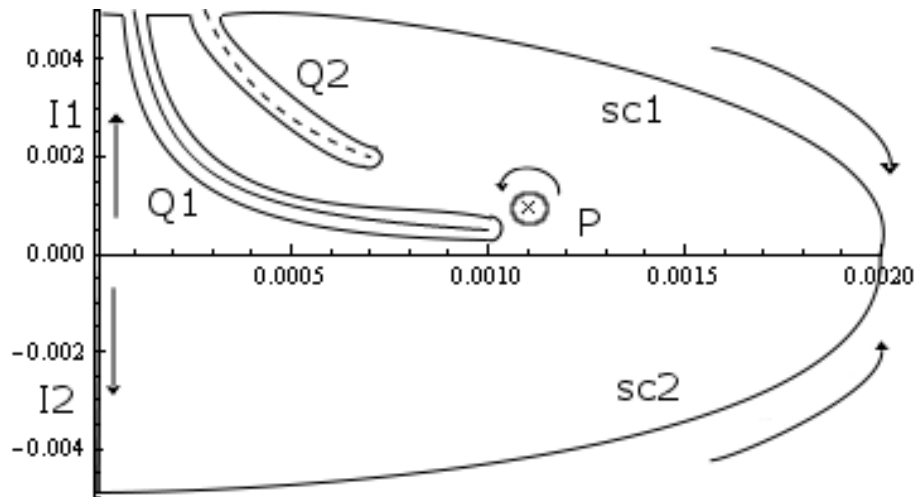


Figure 2.12: Deformation of the integration path according to Sommerfeld's method. The path consisting of I1, Q1, Q2, sc1 and P are part of the deformed  $H^{(1)}$  path. I2 and sc2 are part of the integration path for the  $H^{(2)}$  function

For integration in the complex plane, it is very convenient to perform the integration along a closed contour. From Cauchy's integral theorem

$$\oint_{\gamma} f(z)dz = 2\pi i \sum_{k=1}^n Res(f, a_k),$$

we know that the integration along a closed contour can be replaced by the calculation of the residues at the singular points  $a_k$ . The integration path drawn in Fig. 2.11 can be deformed into a closed contour by using the following identity for the Bessel function [26]

$$J_n(z) = \frac{1}{2}[H_n^{(1)}(z) + H_n^{(2)}(z)]. \quad (2.3.24)$$

The functions denoted by  $H_n^{(1)}$  and  $H_n^{(2)}$  are the  $n^{\text{th}}$  order Hankel functions of the first and second kind. The reason for this substitution is the rapid decay of  $H^{(1)}$  ( $H^{(2)}$ ) in the positive (negative) imaginary half plane. We make use of this property by deforming  $H^{(1)}$  to positive imaginary values and  $H^{(2)}$  to negative imaginary values.

The deformed contour is shown in Fig. 2.12. It should be noticed that the contour has to be deformed on the Riemann sheet where the imaginary parts of both  $k_{1,z}$  and  $k_{2,z}$  are positive and, therefore, the radiation conditions are satisfied.

Using the decay properties of the Hankel functions, the contributions of the parts 'sc1' and 'sc2' will go to zero if the contour will be deformed far enough into the imaginary planes. Furthermore, using the analytic continuation [26]

$$H_n^{(2)}(xe^{-i\pi}) = -H_n^{(1)}(x),$$

it becomes clear that the integrations along 'I1' and 'I2' will cancel each other. Therefore, we are only left with the contributions of the singularity and the branch cuts. Using Cauchy's theorem, we can write

$$\int_0^{\infty} I_{z,z}(k_\rho) dk_\rho - \int_{-Q1, Q2} I_{z,z}(k_\rho) dk_\rho = 2\pi i \text{Res}(I_{z,z}, k_\rho = k_{SPP}) \quad (2.3.25)$$

where  $I_{z,z}$  is the integrand of equation 2.3.21 with  $J_0$  substituted for  $\frac{1}{2}H_0^{(1)}$ . The Hankel function of the second kind can be neglected, since there are no contributions to the electric field that come from the lower imaginary half plane. The integration over '-Q1, Q2' denotes the integration over the contours Q1 and Q2, but in opposite directions. More precisely, the integral from equation 2.3.21 can be rewritten as

$$\begin{aligned} \int_0^{\infty} J_0(k_\rho \rho) \frac{k_\rho^3}{k_{1,z} \epsilon_1 k_{2,z} + \epsilon_2 k_{1,z}} e^{ik_{1,z}(z+h)} dk_\rho &= 2\pi i \text{Res}(k_\rho = k_{SPP}) \\ &+ \int_{+Q1, Q2} \frac{1}{2} H_0^{(1)}(k_\rho \rho) \frac{k_\rho^3}{k_{1,z} \epsilon_1 k_{2,z} + \epsilon_2 k_{1,z}} e^{ik_{1,z}(z+h)} dk_\rho \end{aligned} \quad (2.3.26)$$

The calculation of the Sommerfeld integral is now reduced to calculating the residue at the singularity  $k_\rho = k_{SPP}$  and integration along the branch cuts.



Let us first take a look at the calculation of the residue. The part of the integrand that gives rise to the singularity, is the denominator  $\epsilon_1 k_{2,z} + \epsilon_2 k_{1,z}$ . The residue corresponding to this singularity can easily be calculated, using the following relation

$$\begin{aligned} \frac{dk_\rho}{\epsilon_1 \sqrt{k_2^2 - k_\rho^2} + \epsilon_2 \sqrt{k_1^2 - k_\rho^2}} &= \left[ \frac{d}{dk_\rho} (\epsilon_1 \sqrt{k_2^2 - k_\rho^2} + \epsilon_2 \sqrt{k_1^2 - k_\rho^2}) \right]^{-1} \\ &= - \left[ \frac{\epsilon_1 k_\rho}{\sqrt{k_2^2 - k_\rho^2}} + \frac{\epsilon_2 k_\rho}{\sqrt{k_1^2 - k_\rho^2}} \right]^{-1} \end{aligned}$$

Substituting the above relation in the integrand and substituting  $k_{SPP}$  for  $k_\rho$ , one obtains the residue corresponding to the singularity. Therefore, the electric field contribution coming from the SPP mode in medium 1, is given by

$$E_{SPP,zz} = -\frac{2\pi}{\epsilon_1} H_0^{(1)}(k_{SPP}\rho) \frac{k_{SPP}^2}{\sqrt{k_1^2 - k_{SPP}^2}} \frac{\epsilon_1 \sqrt{k_2^2 - k_{SPP}^2}}{\frac{\epsilon_1}{\sqrt{k_2^2 - k_{SPP}^2}} + \frac{\epsilon_2}{\sqrt{k_1^2 - k_{SPP}^2}}} e^{i\sqrt{k_1^2 - k_{SPP}^2}(z+h)}. \quad (2.3.27)$$

The integration along the contours Q1 and Q2 can be performed by making use of the fact that we defined the branch cuts to be the lines on which the imaginary parts of  $k_{1,z}$  and  $k_{2,z}$  are zero. As an example, the integration along Q1 will be discussed here. We assume the contour Q1 to lie infinitesimally close to the branch cut of  $k_{1,z}$ . On this branch, we can write  $\sqrt{k_1^2 - k_\rho^2} = \tau$ , for real values of  $\tau$ . On the right side of this branch  $\tau$  will be negative and on the left side it will be positive. Looking at Fig. 2.12, this means that we can change the integration of  $k_\rho$  over the contour Q1, into an integration over  $\tau$  from  $\infty$  to  $-\infty$ . In order to do this, we only have to make the following substitutions

$$\begin{aligned} \sqrt{k_1^2 - k_\rho^2} &= \tau, \\ \sqrt{k_2^2 - k_\rho^2} &= \sqrt{k_2^2 - k_1^2 + \tau^2}, \\ k_\rho &= \sqrt{k_1^2 - \tau^2} \quad \text{and} \\ dk_\rho &= \frac{-\tau}{\sqrt{k_1^2 - \tau^2}} d\tau. \end{aligned}$$

Now, the integration over the branch cut Q1 can be performed. A similar treatment can be used for integrating along Q2.

The integration method proposed here is very convenient for separating the different contributions present in the integral. For this project it is especially helpful that the

contribution of the singularity (i.e. the field produced by the SPP-mode at a metal-dielectric interface) can be singled out analytically. There is, however, a big disadvantage of this method: the proposed contour deformation is not possible for  $\rho = 0$ . This implies that exactly below or above the dipole, it is not possible to separate the different contributions. The reason for this is the logarithmic singularity of the Hankel functions at 0. Thus, for calculating the field exactly above or below the dipole, as well as for the calculation of the self-interaction of the dipole via the interface, another integration method needs to be used.

### Integration along an elliptical path

A different method for evaluating the Sommerfeld integrals was proposed by Paulus et al in [23]. Since the main difficulties are on the real axis and in the first quadrant (see Fig. 2.11), they decided to deform the contour into the fourth quadrant and go far enough away from the singularities and branch cuts. Although these features are reflecting the physical phenomena that are present in the problem, the integration path in the fourth quadrant is much smoother and integration along this contour will give an efficient and accurate method for calculating the Sommerfeld-integrals. The integration path is shown in Fig. 2.13. For evaluating this integral along this contour it is not necessary to substitute the Bessel functions for Hankel functions, hence, there is no fundamental problem for performing the integration for  $\rho = 0$ . However, some small changes have to be made to the integrands for calculating at  $\rho = 0$ . These integrands are given in the appendix.

## 2.4 Green's tensor formalism

In the previous sections, it was discussed what SPP modes are and how they can be excited, how metal nanoparticles respond to an electric field and how the electric field of an oscillating dipole close to a metal can be calculated. The aim of this project, however, is to study the excitation and propagation of SPP modes by an array of metal nanoparticles. Therefore, we need a method to describe the coupling between the individual metal nanoparticles and their response in the proximity of a metal.

The method to be used for these sort of problems, is the Green's tensor formalism. The Green's tensor  $\mathbf{G}(\mathbf{r}, \mathbf{s})$  represents the electric field radiated at an arbitrary point  $\mathbf{r}$  by three orthogonal dipoles at a source point  $\mathbf{s}$ . The tensor component  $G_{i,j}$  represents the

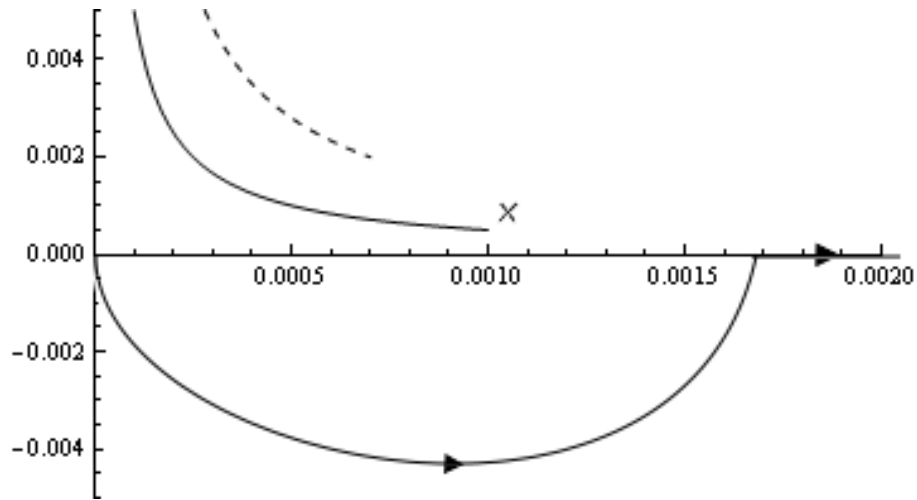


Figure 2.13: The integration path for evaluating Sommerfeld-integrals using the method proposed by Paulus et al [23].

$j$ -component of the electric field, produced by a dipole oscillating in the  $i$ -direction:

$$\mathbf{G}(\mathbf{r}, \mathbf{s}) = \begin{pmatrix} G_{x,x}(\mathbf{r}, \mathbf{s}) & G_{x,y}(\mathbf{r}, \mathbf{s}) & G_{x,z}(\mathbf{r}, \mathbf{s}) \\ G_{y,x}(\mathbf{r}, \mathbf{s}) & G_{y,y}(\mathbf{r}, \mathbf{s}) & G_{y,z}(\mathbf{r}, \mathbf{s}) \\ G_{z,x}(\mathbf{r}, \mathbf{s}) & G_{z,y}(\mathbf{r}, \mathbf{s}) & G_{z,z}(\mathbf{r}, \mathbf{s}) \end{pmatrix}$$

For example, in the present case, the component  $G_{x,x}(\mathbf{r}, \mathbf{s})$  denotes the  $x$ -component of the oscillating electric field at the point  $\mathbf{r}$  produced by a dipole oscillating in the  $x$ -direction at the source point  $\mathbf{s}$ , in the presence of a reflecting interface.

As was discussed in section 2.3 the electric field of a dipole oscillating close to an interface, can be written as the sum of the homogeneous field and the field scattered from the interface. Since, the Green's tensor consists of these electric field components, it can be split in a similar fashion, that is

$$\mathbf{G}(\mathbf{r}, \mathbf{s}) = \mathbf{G}^H(\mathbf{r}, \mathbf{s}) + \mathbf{G}^S(\mathbf{r}, \mathbf{s}).$$

Here  $\mathbf{G}^H$  refers to the Green's tensor in a homogeneous environment, i.e. no interface present. All contributions to the field coming from the interface, are contained in  $\mathbf{G}^S$ .

From section 2.2 we know that the dipole moment of a metal nanoparticle is proportional to the electric field 'felt' by the particle. For an array of particles, this implies that the dipole moment of a certain particle is determined by the field radiated by all the other particles. An important assumption is that only the first dipole is excited by an external

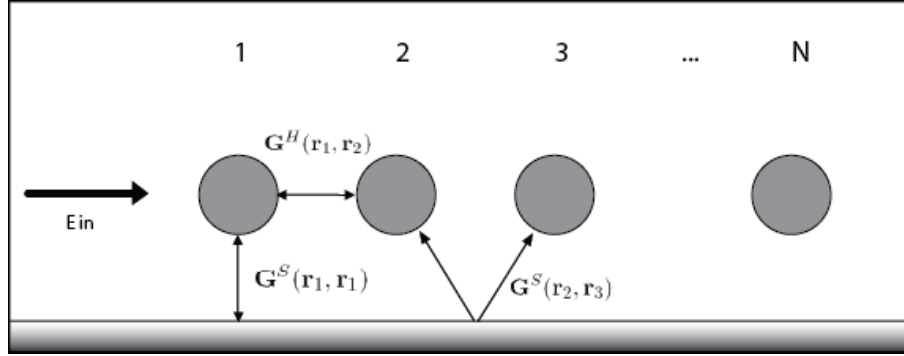


Figure 2.14: The interactions that are present for an array of MNPs close to a reflecting interface

field and a continuous wave excitation is considered. Under these conditions, we can write down the steady state equations of motion for the system:

$$\mathbf{p}_1 = \alpha_1 \mathbf{E}_0(\mathbf{r}_1) + \frac{k_0^2}{\epsilon_0} \alpha_1 \mathbf{G}^S(\mathbf{r}_1, \mathbf{r}_1) \mathbf{p}_1 + \frac{k_0^2}{\epsilon_0} \sum_{j \neq 1}^N \alpha_1 [\mathbf{G}^H(\mathbf{r}_1, \mathbf{r}_j) + \mathbf{G}^S(\mathbf{r}_1, \mathbf{r}_j)] \mathbf{p}_j, \quad (2.4.1)$$

$$\mathbf{p}_i = \frac{k_0^2}{\epsilon_0} \alpha_i \mathbf{G}^S(\mathbf{r}_i, \mathbf{r}_i) \mathbf{p}_i + \frac{k_0^2}{\epsilon_0} \sum_{j \neq i}^N \alpha_i [\mathbf{G}^H(\mathbf{r}_i, \mathbf{r}_j) + \mathbf{G}^S(\mathbf{r}_i, \mathbf{r}_j)] \mathbf{p}_j, \quad i = 2, \dots, N. \quad (2.4.2)$$

In these equations,  $\mathbf{p}_i$  is the dipole moment,  $\alpha_i$  the polarizability and  $\mathbf{r}_i$  the position of the  $i^{th}$  particle.  $E_0$  is the external electric field vector with the direction determined by the polarization and the magnitude by the field strength. If all particles would be excited, equation 2.4.2 would contain an extra  $\alpha_i \mathbf{E}_{i,0}$  term and the summation would be running from 1 to  $N$ .

The system of equations 2.4.1 and 2.4.2 has to be solved in order to obtain the dipole moments of all particles and be able to calculate the total electric field produced by these particles. For the latter, the following formula can be used

$$\mathbf{E}(\mathbf{r}) = \frac{k_0^2}{\epsilon_0} \sum_{i=1}^N [\mathbf{G}^H(\mathbf{r}, \mathbf{r}_i) + \mathbf{G}^S(\mathbf{r}, \mathbf{r}_i)] \mathbf{p}_i. \quad (2.4.3)$$

The equations given above are the same as used by Bozhevolnyi et al in [11] to calculate the electric field produced by an array of gold particles close to a gold surface.

# Chapter 3

## Results and Discussion

### 3.1 One metal nanoparticle close to a metal half-space

Using Sommerfeld's method, outlined in section 2.3, we will now study the electric field of a metal nanoparticle close to a metal half-space. In this report we chose to focus on silver nanospheres embedded in glass and close to a silver half-space. It is important to note that the treatment is valid for any kind of material, as long as the permittivity of the material is known. To describe the permittivity of silver, we use the generalized Drude model [12]

$$\epsilon_{silver}(\omega) = 5.46 - 0.73 \frac{(1.72 \cdot 10^{16})^2}{\omega^2 + i8.35 \cdot 10^{13}\omega}, \quad (3.1.1)$$

which is an extension of the 'normal' Drude model in order to match the experimental data better. For the surrounding glass (medium 1), we will use  $\epsilon_1 = \epsilon_{glass} = 2.25$ . The polarizability of the metal nanosphere will be calculated from

$$\frac{1}{\alpha} = \frac{1}{\alpha^{(0)}} - \frac{k^2}{a} - \frac{2i}{3}k^3, \quad \text{where} \quad \alpha^{(0)} = 4\pi a^3 \frac{\epsilon - \epsilon_m}{\epsilon + 2\epsilon_m}. \quad (3.1.2)$$

The dipole moment of a single nanosphere is determined by the external field and the self-interaction of the particle via interface and therefore can be calculated from the first two terms of equation 2.4.1. For this calculations continuous excitation is assumed and therefore the steady-state response will be calculated.

Using the equations obtained from Sommerfeld's treatment, we can now calculate the electric fields of a silver nanosphere (embedded in glass) close to a silver half-space as is shown in figures 3.1(a) and 3.1(b). In these figures the absolute value of the total electric

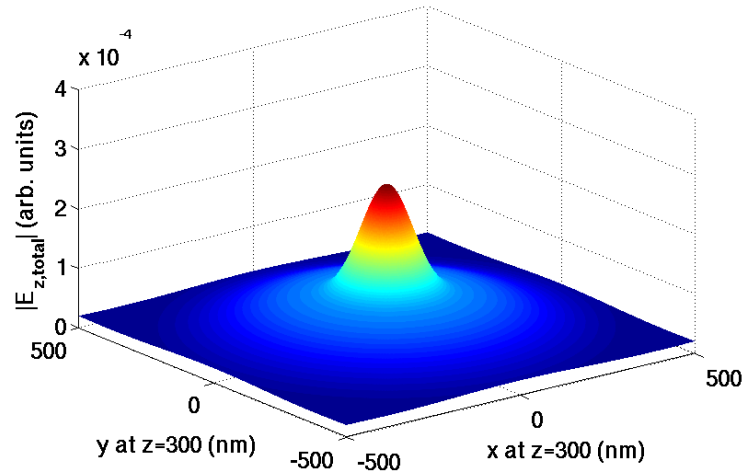
field, calculated from equation 2.3.21, and the absolute value of the electric field produced by the surface plasmon polaritons, calculated using equation 2.3.27, are shown. As should be expected from the equations of the fields, the electric field is cylindrically symmetric, with a maximum intensity at the cylinder axis ( $\rho = 0$ ). Looking carefully at these graphs, one can observe that the intensity of the field produced by the SPPs at  $\rho = 0$  is higher than the total field. This fact can be understood by looking at the different contributions to the field in more detail.

For these types of systems, the electric field can be split up in 5 different contributions:

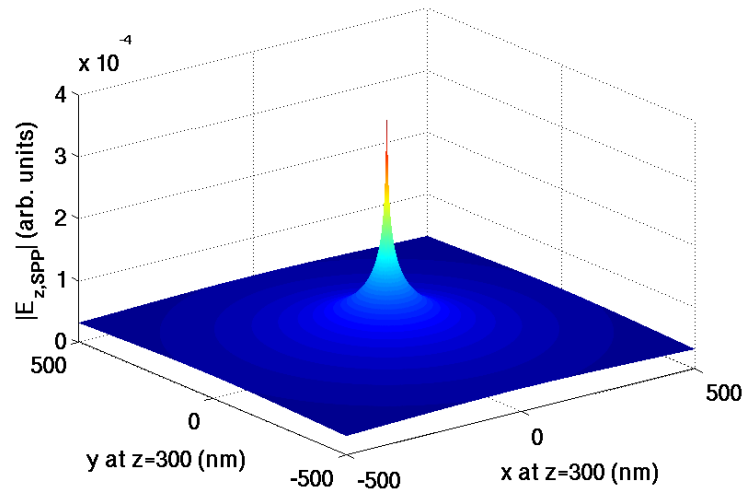
1. Direct contribution: Electric field as if no interface is present
2. Image contribution: Field reflected from the interface, assuming a perfect reflector
3. s-modes: Fields decaying exponentially from the interface with s (also TE) polarization
4. p-modes: Fields decaying exponentially from the interface with p (also TM) polarization
5. SPP-mode: p-mode with the wave-vector that matches the bound surface mode wavevector given by equation. 2.1.10

For a single particle close to a partially reflecting interface that is excited with a  $z$ -polarized beam, the dipole moment will only have a  $z$ -component. This implies that the dipole moment of the particle will be oscillating perpendicular to the interface and therefore no modes with s-polarization (i.e. in-plane polarization) will be excited. As was shown in section 2.3.3, the integration of the p-component can be split into the calculation of the residue of the singularity and integration along the branch cuts. Since the singularity corresponds to the bound surface mode, we will be referring to this field as the SPP mode. The contribution of the remaining integration will be referred to as the p-modes. Using the elliptical integration path, outlined in the same section, the contribution of all p-polarized surface modes can be calculated.

Figure 3.2 shows the SPP and the p-mode contribution to the electric field under the same conditions as in Fig. 3.1(a), but now with  $y = 0 \text{ nm}$ . It is interesting to see that at  $\rho = 0$  both the SPP and p-mode contributions reach a maximum. However, the sum of these two contributions does not. This implies that the maximum of the SPP is partially



(a) Total field



(b) SPP contribution

Figure 3.1:  $z$ -component of the electric field produced by a silver nanoparticle ( $a = 50 \text{ nm}$ ) at a distance  $h = 150 \text{ nm}$  from a silver half-space. The excitation is  $z$ -polarized and with a wavelength in glass of  $422 \text{ nm}$ . The field is calculated at a distance of  $z = 300 \text{ nm}$  above the interface.

compensated by the other  $p$ -modes with an opposite phase. This is necessary, because due to the presence of the Hankel function in the equation for the field produced by the SPPs, this field actually becomes infinite at  $\rho = 0$ , which is unphysical.

Comparing figure 3.2 and 3.3 shows that the decay into the glass for SPP and  $p$ -modes

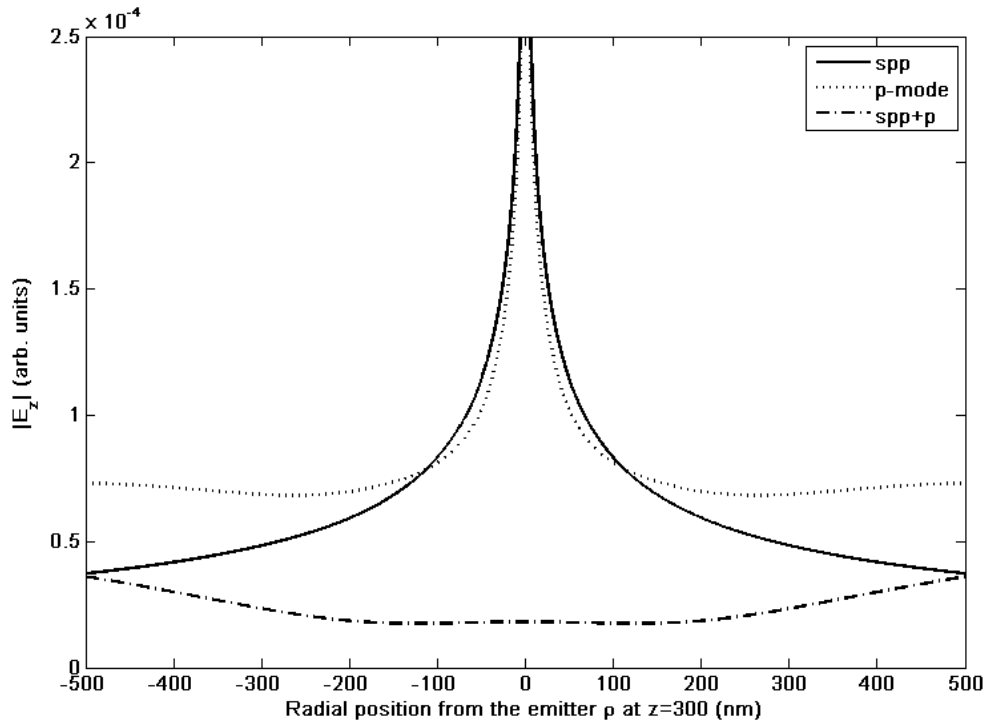


Figure 3.2: The SPP and the p-field produced by a silver nanoparticle ( $a = 50 \text{ nm}$ ), embedded in glass at a height  $h = 150 \text{ nm}$  above a silver half-space. The field is calculated at a distance  $z = 300 \text{ nm}$  above the interface. It can be clearly seen that whereas both the SPP and the p mode have a maximum for  $\rho = 0 \text{ nm}$ , their maxima partially compensate when they are added up.

is quite different. At  $z = 300 \text{ nm}$  the field of the p-modes is stronger than that of the SPPs if  $|\rho| > 100 \text{ nm}$ , whereas for  $z = 0 \text{ nm}$  the SPP contribution is the largest for all values of  $\rho$ .

Another feature that can be seen from the above figures, is that the decay of the SPP-mode appears to be stronger than that of the total field and also faster than exponential, as should be expected from Maxwell's equations (see section 2.1). The reason for this is that in the derivation from Maxwell's equations, we assumed propagation in one dimension. In the present case, the SPP is actually propagating over a two dimensional interface. This can be clearly seen by looking at the asymptotic expansion of the Hankel function [26]

$$H_0^{(1)}(k_\rho \rho) = \sqrt{\frac{2}{\pi k_\rho \rho}} e^{i(k_\rho \rho - \pi/4)}.$$



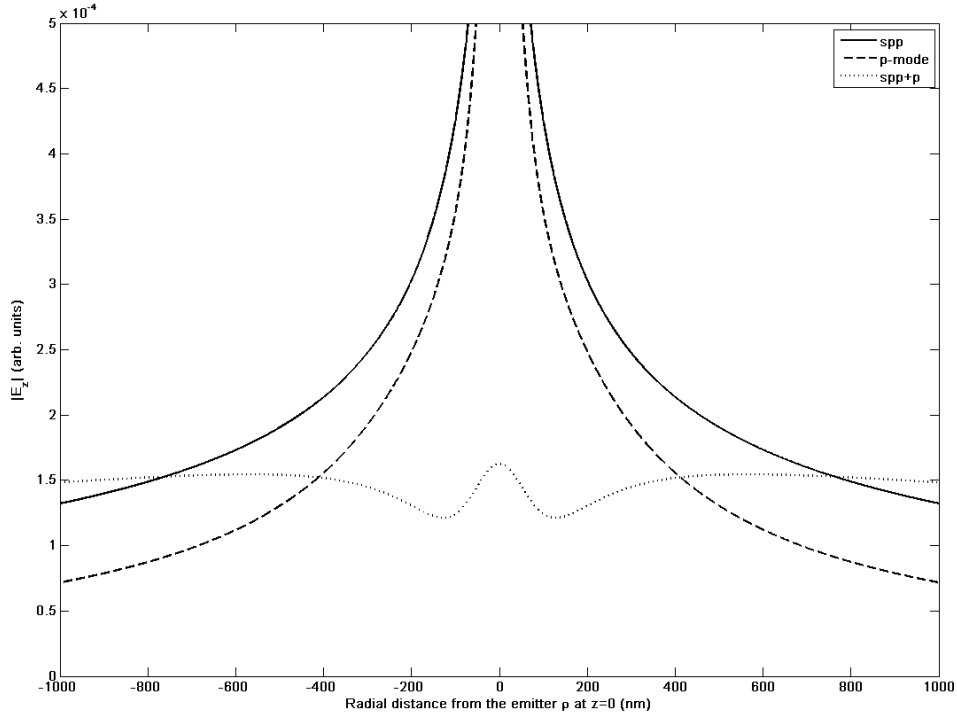


Figure 3.3: The SPP and the p-field produced by a silver nanoparticle ( $a = 50 \text{ nm}$ ), embedded in glass at a height  $h = 150 \text{ nm}$  above a silver half-space. The field is calculated at a distance  $z = 0 \text{ nm}$  above the interface. It can be clearly seen that whereas both the SPP and the p mode have a maximum for  $\rho = 0 \text{ nm}$ , their maxima partially compensate when they are added up.

Inserting this in the expression for the field corresponding to SPP modes (equation 2.3.27), we obtain

$$|E_{SPP,zz}| \propto \sqrt{\frac{1}{|k_\rho|\rho}} e^{-Im[k_\rho]\rho}, \quad (3.1.3)$$

that is, there is an extra  $\rho^{-1/2}$  factor present. This factor can be interpreted by thinking of the energy dissipation. The energy is proportional to the square of the electric field. Therefore, a factor  $\rho^{-1}$  will be present in the energy. This factor can be thought as the energy dissipation through the circumference of a circle on the interface, which is two dimensional dissipation.

As was suggested in section 2.3.2, the energy dissipated into the SPP mode depends

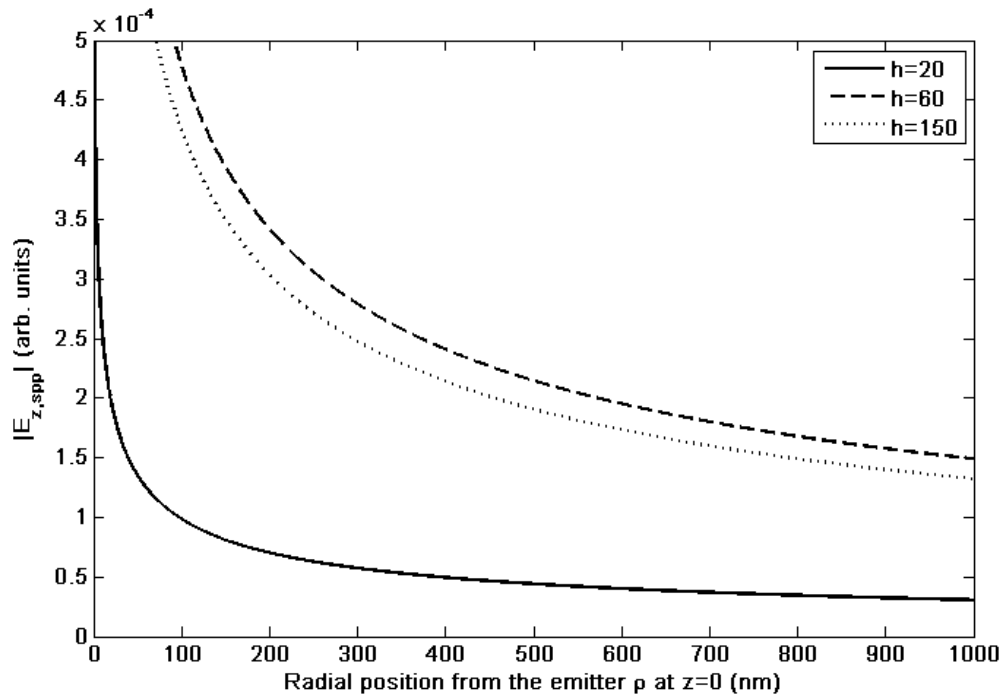


Figure 3.4: Absolute value of the  $z$ -component of the electric field produced by SPP modes on a silver/glass interface by a silver nanosphere ( $a = 50 \text{ nm}$ ) at various heights above the interface. The sphere is excited by a  $z$ -polarized beam with a wavelength in glass of  $422 \text{ nm}$ .

on the distance between the emitter and the interface. For very small separations the coupling to the so-called 'lossy surface waves' becomes an important decay channel and therefore there is an optimum coupling distance for exciting SPPs. This is also illustrated in figure 3.4. From this graph it is clearly visible that the electric field produced by a nanosphere at  $h = 60 \text{ nm}$  is larger than if the particle is positioned at  $h = 20 \text{ nm}$  or  $h = 150 \text{ nm}$ . It is important to note that for very small separations, the validity of the dipole approximation for the metal nanoparticle becomes doubtful. According to the authors of [12], the dipole approximation for nanospheres is valid, as long as the radius of the particles is smaller than one third of the center-to-center distance. Since in this case the sphere is interacting with itself via the interface, we will assume here that it is allowed to only consider dipole contributions if the separation between the (point) dipole and the interface is larger than 1.5 times the radius. Figure 3.4 should therefore just be considered as a qualitative illustration of the physical effect.

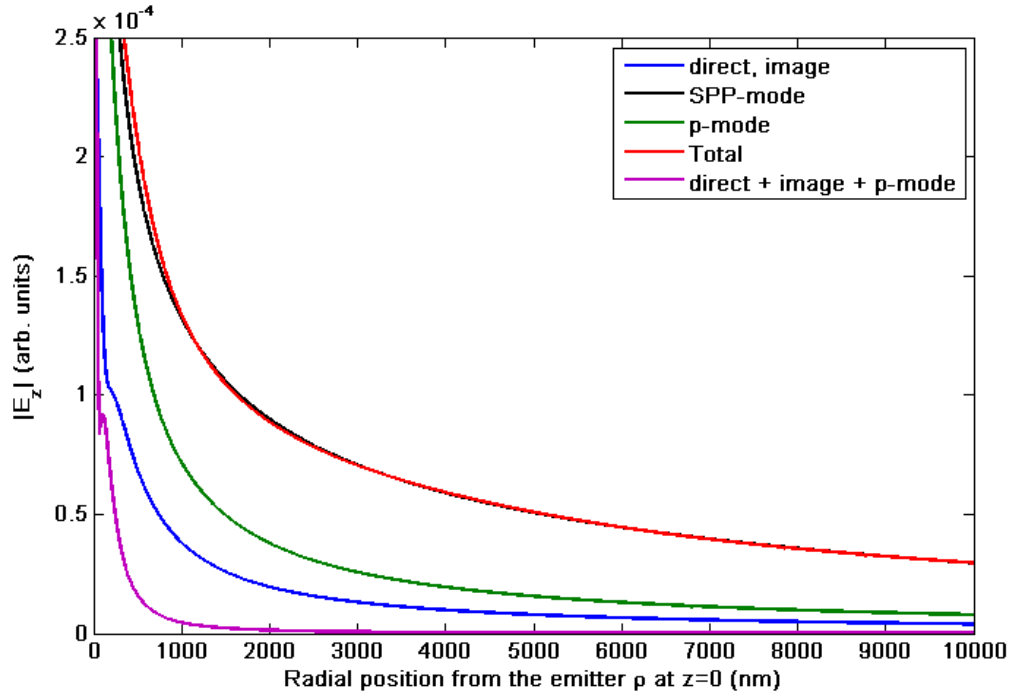


Figure 3.5: Absolute value of the  $z$ -component of the electric field on a silver/glass interface ( $z = 0$  nm) produced by a silver nanosphere ( $a = 50$  nm) at  $150$  nm above the interface. The sphere is excited by a  $z$ -polarized beam with a wavelength in glass of  $422$  nm. It can be clearly seen that for  $\rho > 2500$  nm the (analytical!) SPP curve matches the total field exactly.

We will conclude this chapter by showing the different electric field contributions as a function of  $\rho$ . In figure 3.5 the different contributions at the interface ( $z = 0$ ) are displayed. Since the interface is exactly in between the source and the induced image dipole, the contributions of these terms are equal and are shown as the blue line. It is interesting to observe the similarity between the total field and the field produced by the SPPs. Especially for  $\rho > 2500$  the difference is very small. Also plotted is the sum of the direct field, the field coming from the image dipole and the  $p$ -modes. Interestingly, they are partially canceling each other and therefore have almost no contribution to the far field.

## 3.2 An array of metal nano-particles close to a metal surface

In the previous section, we have seen that a surface plasmon polariton mode excited by one metal nano-particle suffers from severe decay. This is due to the fact that the polariton is decaying over the interface, i.e. in two dimensions.

In view of applications in opto-electronics, it is important that these SPP modes can be guided precisely and over a sufficient distance for on-chip communication. A possible technique for this is to guide SPPs by an array of nano-particles above a metal-dielectric interface, as was shown by [11]. The reasoning behind this geometry is that the dipole-dipole coupled metal-nanoparticles form an efficient path for energy transport. Throughout this section an array of  $N$  silver nano-spheres (radius  $a = 50$  nm), with a center-to-center distance  $d$  and at a height of  $h$  above a silver half-space. The permittivity of the silver spheres and the half-space will be determined using the generalized Drude model given in equation 2.1.13. The array is embedded in glass with a dielectric constant of  $\epsilon_{glass} = 2.25$ . Only the first nano-particle will be excited. The excitation beam is polarized perpendicular to the interface (i.e.  $z$ -polarization) and the first particle will be irradiated continuously. Therefore, we are calculating the steady state response of the system.

As stated earlier, in view of applications, it is of particular importance to understand the decay behavior of the electric field guided by such a system. To this end, we will first calculate the dipole moments of the nano-spheres and study the decay length as a function of the excitation wavelength  $\lambda$ , the center-to-center distance  $d$  and the height  $h$  of the array above the surface. After these effects are known, the electric field that is produced on the interface by such an array will be calculated. Using this field, we will show that the array can have both constructive and destructive effects on the decay length. Finally, it will also be shown that the main contribution to the field produced on the interface by an array, is the field produced by the surface plasmon polaritons.

### 3.2.1 Dipole moments of metal nano-particles in an array close to an interface

As was explained in section 2.4, equations 2.4.1 and 2.4.2 need to be solved for the calculation of the dipole moments. For an array of  $N$  equidistant and identical particles, these equations can be simplified quite a bit. Since all particles are identical, their polarizabilities are also identical, i.e.  $\alpha_i = \alpha$ . Furthermore, if the center-to-center distance ( $d$ ) of

the particles in the array is identical, than  $\mathbf{G}(\mathbf{r}_1, \mathbf{r}_2) = \mathbf{G}(\mathbf{r}_2, \mathbf{r}_3)$  and  $|\mathbf{r}_i - \mathbf{r}_j| = d \cdot |i - j|$ . Using these assumptions, the dipole moment can be determined by solving the following equation

$$\begin{pmatrix} \mathbf{p}_1 \\ \mathbf{p}_2 \\ \cdot \\ \cdot \\ \mathbf{p}_N \end{pmatrix} = \begin{pmatrix} \mathbf{G}(0,0) - \alpha & \mathbf{G}(0,d) & \cdot & \cdot & \mathbf{G}(0,(N-1)d) \\ \mathbf{G}(0,d) & \mathbf{G}(0,0) - \alpha & \cdot & \cdot & \mathbf{G}(0,(N-2)d) \\ \cdot & \cdot & \cdot & \cdot & \cdot \\ \cdot & \cdot & \cdot & \cdot & \cdot \\ \mathbf{G}(0,(N-1)d) & \cdot & \cdot & \cdot & \mathbf{G}(0,0) - \alpha \end{pmatrix}^{-1} \begin{pmatrix} -\mathbf{E}_0 \\ 0 \\ \cdot \\ \cdot \\ 0 \end{pmatrix}.$$

In this equation,  $\mathbf{p}_i$  is the vector representing the dipole moment of particle  $i$  and  $\mathbf{G}(0, s)$  is the Green's tensor of a dipole situated at 0, creating an electric field at the point  $s$ . The tensor  $\mathbf{G}(0,0)$  is the Green's tensor corresponding to the self-interaction of the emitter via the interface.

Figure 3.6 shows a result that is typical for an array close to a partially reflecting surface. Presented are the absolute values of the  $x$  and the  $z$ -components of the dipole

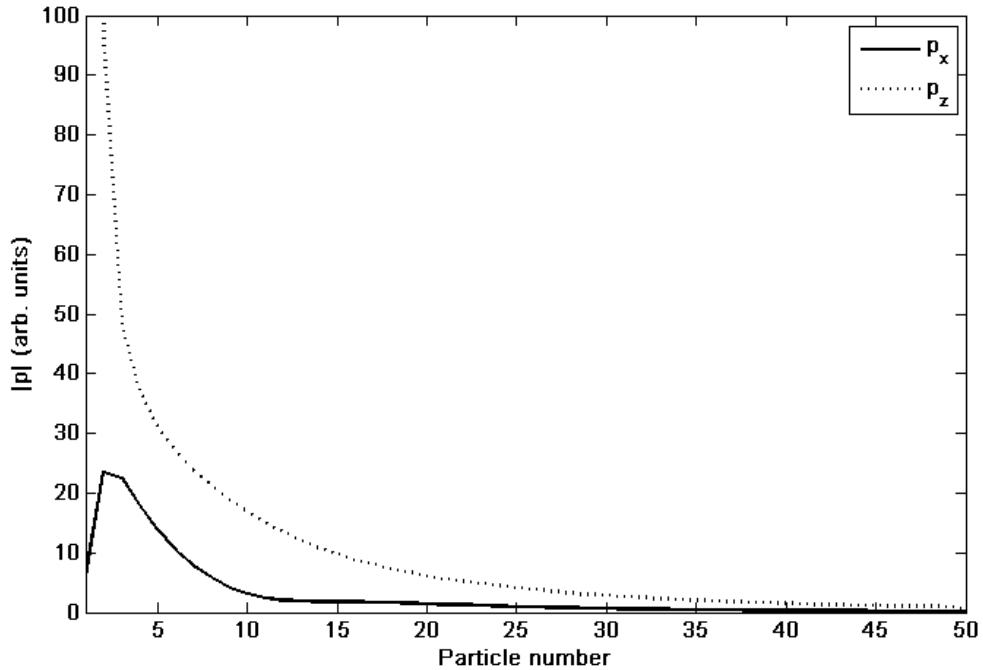


Figure 3.6: Absolute values of the dipole moments in an array of 50 identical silver nanospheres. The excitation is  $z$ -polarized.

moments for each particle in the array. If the excitation is assumed to be  $z$ -polarized, the  $x$  components of the dipole moments will be much smaller. The reason for this is that the only way for a particle to acquire an  $x$ -component, is via reflection of the fields of neighboring particles at the interface. Since the first particle has less neighboring particles than the second and the third, the  $x$ -component increases first. After the first few particles, the losses make the dipole moments decrease again. Because in this project we consider continuous excitation, the  $z$ -component of the dipole moment of the first particles is very high compared to particles further down the array.

Due to the rapid decrease of the  $z$ -component at the beginning of the array, the usual  $e^{-1}$ -decay length is not very insightful for this problem, since the decay length then would not extend more than five particles. This means that it will be very hard to investigate the influence of, for example, the inter-particle spacing. Therefore, we decided to look at which particle the dipole moment has decayed to 1% of the value of the first particle. Having defined a proper decay length convention, we are in the position to study the influence of the interface on the decay properties. Specifically, we will investigate the influence of the excitation wavelength on the decay length of the dipole moments, for an array with a given center-to-center distance ( $d$ ) and height above the interface ( $h$ ).

To this extent, we will first calculate the decay length for an isolated array. This is shown in Fig. 3.7. A first feature to notice, is the decreasing decay length for increasing inter-particle spacing. Realizing that, although the electric field of an oscillating dipole has different behavior in different regimes (far field, near field [19]), they all decay as a function of  $R$ . This implies that the further apart the dipoles are, the weaker their coupling will be. Hence, the energy transport along the chain will be worse, which results in a lower decay length. Another feature is the shift of the maximum propagation to the blue part of the spectrum. Comparing the calculation for an isolated array, with those of an array close to a perfect reflecting interface and a silver half-space (figures 3.9 and 3.11, respectively), one notices that the blue-shift is an intrinsic feature of the dipole array and should therefore be related to the dipole-dipole interactions in the particle chain. Looking carefully at the positions of the maxima in Fig. 3.7, it can be observed that the maxima occurs at an integer value times the center-to-center distance  $d$ . To find out the exact cause of this shift, the inter-particle interactions need to be studied in detail.

A large influence of the interface can be found, when comparing the calculations for the isolated array and the array close to a perfect reflector. In the proximity of the interface,

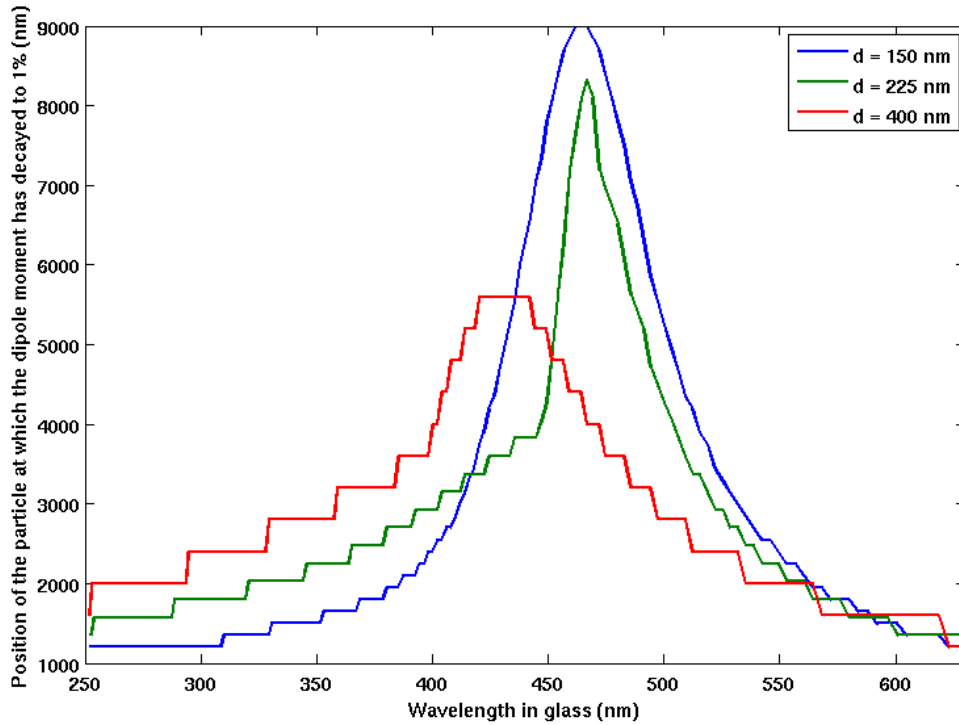


Figure 3.7: The 1%-decay length of the  $z$ -component of the dipole moments is given as a function of the excitation wavelength in the glass. An array of silver nano-spheres ( $a = 50$  nm) and with various center-to-center distances ( $d$ ) is considered in a homogeneous surrounding, i.e. no interface present.

the decay length can be more than doubled. This implies that the reflected field greatly benefits the energy transport through a chain of dipoles. This can be explained by the fact that part of the radiation that would otherwise have been lost, is now reflected back

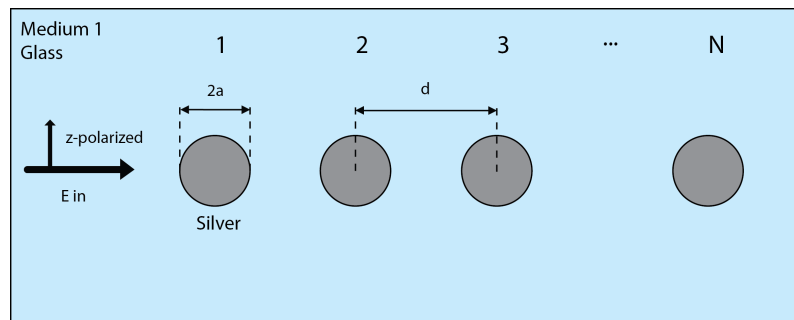


Figure 3.8: Geometry under consideration for the calculation of the dipole moments of MNPs in an isolated array.

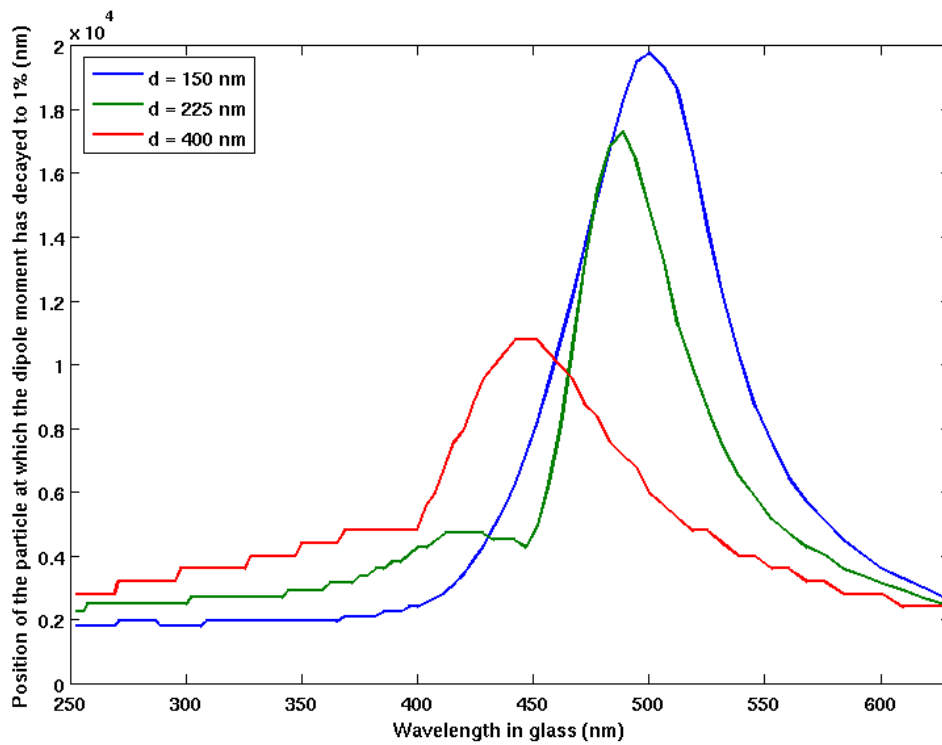


Figure 3.9: As in Fig. 3.7. Now the array is positioned  $h = 150$  nm above a perfect reflector. Only the direct field and the field of the image dipole contribute, see section 2.3.1.

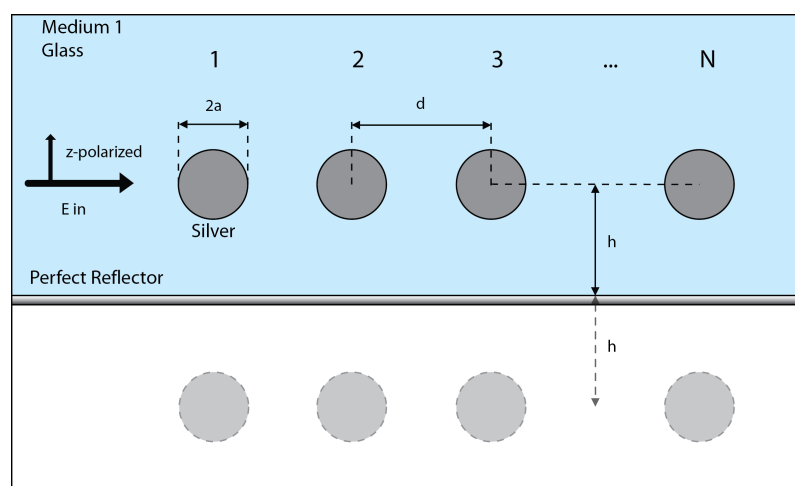


Figure 3.10: Geometry under consideration for the calculation of the dipole moments of MNPs in an array close to a perfect reflector.



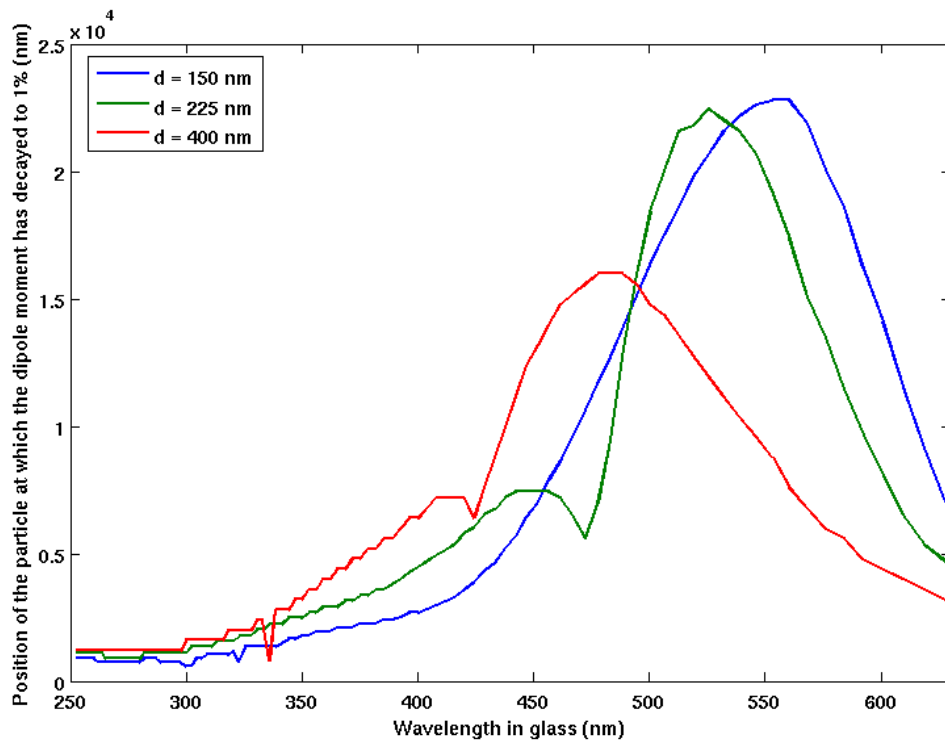


Figure 3.11: As in Fig. 3.9, but now silver is considered instead of a perfect reflection half-space. For this calculation the Sommerfeld integrals need to be solved.

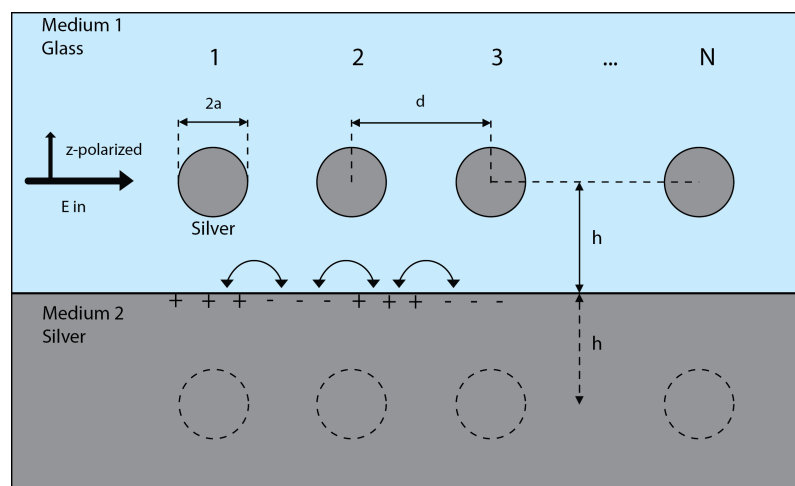


Figure 3.12: Geometry under consideration for the calculation of the dipole moments of MNPs in a real metal.

onto the chain. Effectively this reduces the losses. Another feature that can be noticed when comparing these graphs is the redshift of the maxima in Fig. 3.9. An explanation for this lies in the interaction the array has with the image array (see Fig. 3.10). It is well known that the interaction between two parallel dipoles gives rise to a shift to lower oscillation frequencies, i.e. to the red of the spectrum. This can be shown by using the following equation [19, p. 151]

$$W_{1,2} = \frac{\mathbf{p}_1 \cdot \mathbf{p}_2 - 3(\mathbf{n} \cdot \mathbf{p}_1)(\mathbf{n} \cdot \mathbf{p}_2)}{|\mathbf{x}_1 - \mathbf{x}_2|^3} \quad (3.2.1)$$

From this it can be calculated that for the  $z$ -components of the dipole moments of the MNPs, the sign of the interaction will be negative and therefore a redshift will occur. However, it should be noted that the  $R^{-3}$  only holds for near-field interactions and the interaction between the array and the images is not really part of the near-field, but is very close to it. Therefore, although this explanation is consistent with the observations (see also Fig. 3.13 for  $h$  dependence), the interactions that are present need to be studied in detail to give full explanation.

A perfect reflector is not penetrable for the electric field, therefore the complete field will be reflected. A real material, however, will always allow some field penetration. This leads to surface currents induced at the interface between, in our case, silver and glass. These surface modes can be calculated by using the Sommerfeld integrals, derived earlier in this text. Please note that although the integration runs over all in-plane wave-vectors, only the wavevector corresponding to the surface plasmon polariton (SPP) mode will be the one that is confined to the interface and propagating along it. The influence of these surface modes on the energy transport through the array of nano-particles, can be investigated by looking for the differences between the calculations for an array close to the perfect reflector (Fig. 3.9) and close to the silver half-space (Fig. 3.11). Again, the observation can be made that the decay length is enhanced for all three curves. However, now the increase is not the same for all distances between the particles. The line corresponding to  $d = 150$  nm has the smallest increase and for  $d = 400$  nm the increase is the largest. This effect can be explained by the influence of the SPP. From the dispersion relation for the SPP, equation 2.3.22, one can calculate the wavelength of the SPP corresponding to a certain excitation frequency. The maximum for the  $d = 400$  nm curve, appears to correspond to 1.2 times the corresponding SPP wavelength and for  $d = 225$  nm at 2.2 times the SPP wavelength. The  $d = 150$  nm curve obtains the maximum, however, at a SPP wavelength

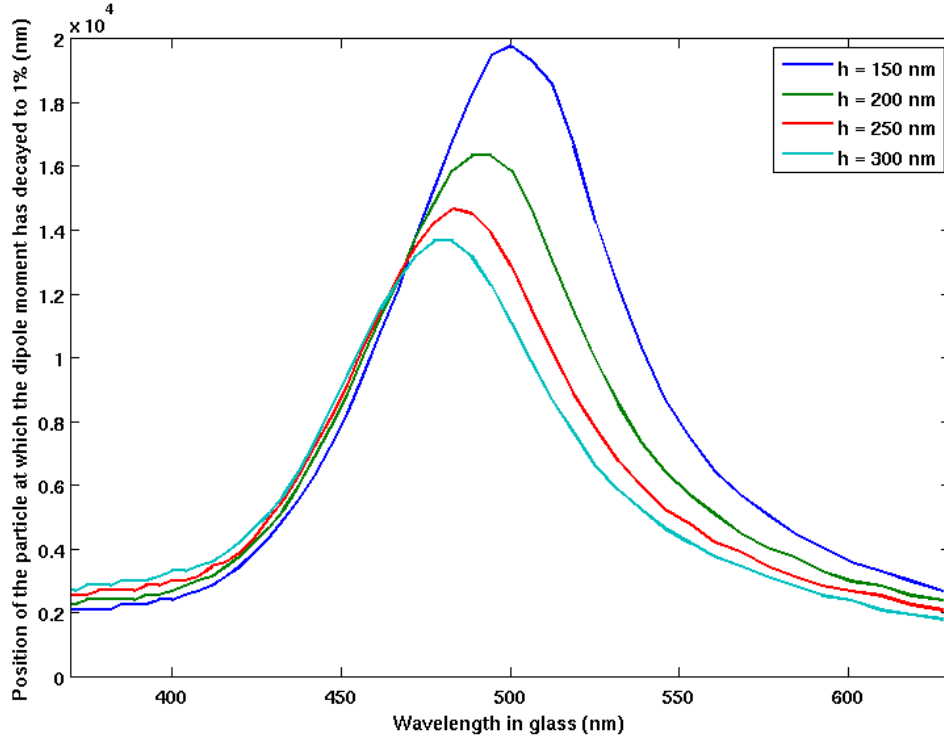


Figure 3.13: As in Fig. 3.9, but now the center-to-center distance is kept constant ( $d = 150$  nm) and the height above the perfectly reflecting interface is varied.

of  $3.67 \cdot d$ . This implies that the plasmon mode would interact with the array of nano-particles more coherently for  $d$  is 225 and 400 nm, than for  $d = 150$  nm. Therefore, the presence of Surface Plasmon Polaritons on the interface increases the energy transport through a chain of MNPs, depending on how the inter-particle spacing matches the SPP wavelength. The small local maximum that occurs to the left of the maximum for inter-particle spacings of 225 and 400 nm, can be explained as an interference effect, because the wavelength corresponding to the peak equals an integer amount the inter-particle spacing.

To check the consistency of the results, we show the decay length as a function of the height above the interface in Fig. 3.13. From this it becomes obvious that the decay length increases with decreasing distance to the interface. Also, extrapolation of the data to larger  $h$ , would lead to a maximum decay length close to  $10\mu\text{m}$ , obtained at  $\lambda$  around 470 nm, i.e. the blue curve in Fig. 3.7.

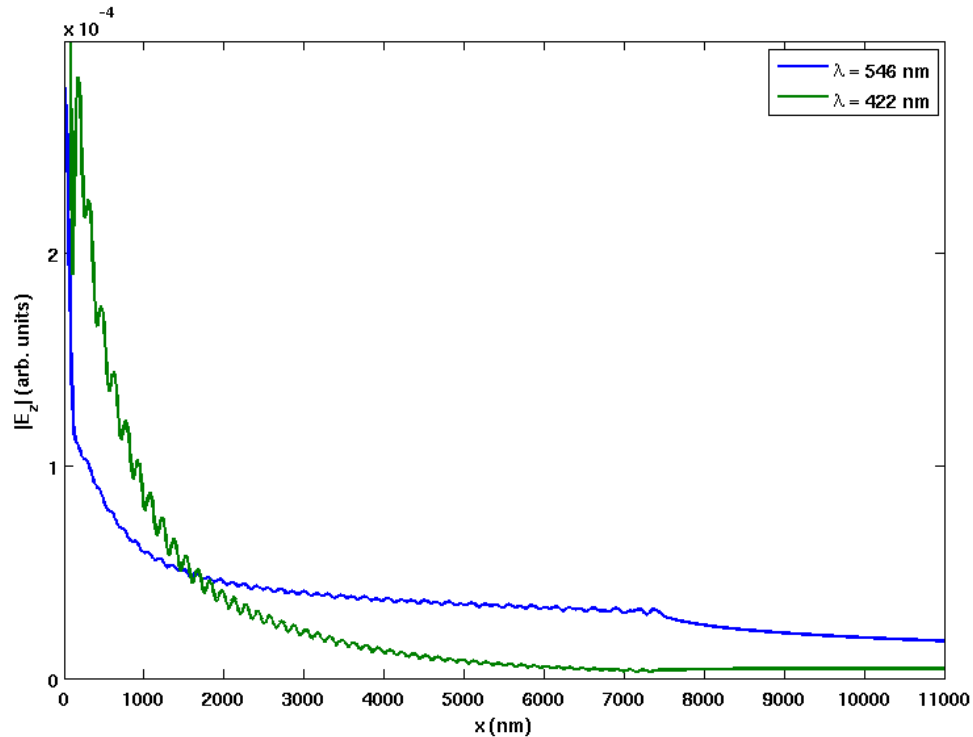


Figure 3.14: The absolute value of the  $z$ -component of the electric field produced at the interface ( $z = 0$ ) by an array of 50 silver nano-spheres ( $a = 50$  nm), with inter-particle distance of  $d = 150$  nm and a height of  $h = 150$  nm above a silver half-space. The difference between the decay length for different excitation wavelengths is clearly visible.

### 3.2.2 Electric field produced by an array of metal nano-particles

In the above section, it was shown that the presence of a (partially) reflecting interface can increase the decay length of the dipole moments. Therefore, energy transport through a chain of metal nano-particles can be improved by adding a (partially) reflecting surface. In this subsection, we will show that increasing the decay length of the dipole moments in an array will not necessarily increase the propagation of the electric field induced at the interface. The motivation behind calculating the field at the interface, is because the SPP mode propagates along this interface. By calculating the field at the interface, it can be investigated if it is possible to extend the propagation of the SPP, while maintaining the sub-wavelength confinement.

In Fig. 3.14 the electric fields produced by two identical arrays of silver nano-particles are shown. Clearly visible is the difference in response for different excitation wavelengths.

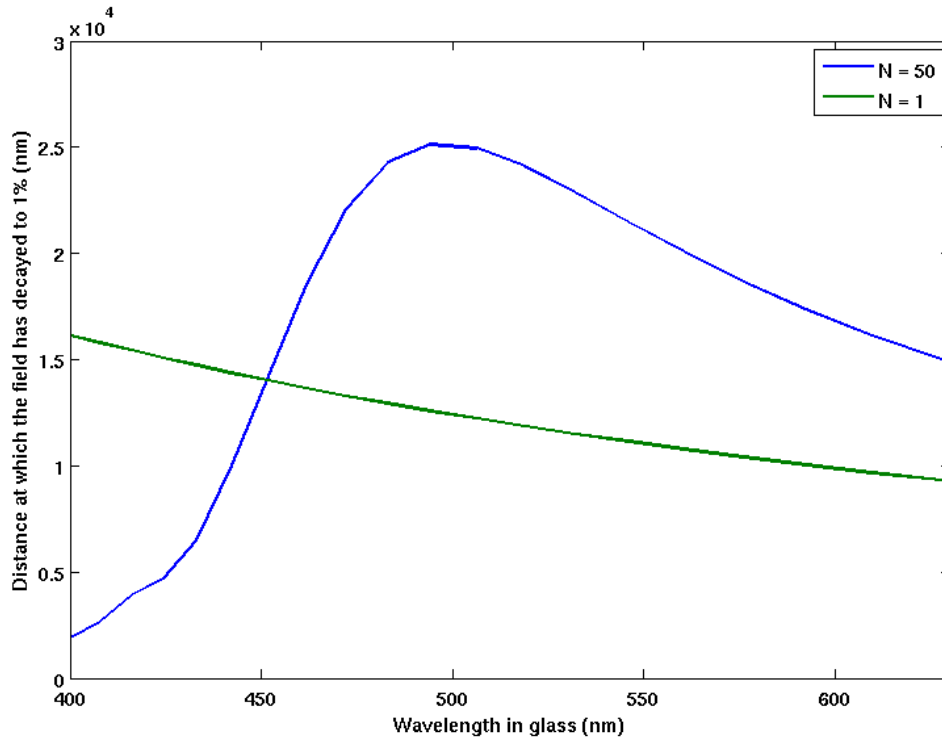


Figure 3.15: Decay length of an array of 50 silver nano-spheres ( $a = 50$  nm), with inter-particle spacing  $d = 150$  nm and a height of  $h = 150$  nm above perfectly reflecting interface. For comparison also the decay length for a single particle under the same conditions is shown.

The wavelength  $\lambda = 422$  nm corresponds to the plasmon resonance in the silver nano-spheres with a radius of  $a = 50$  nm. At this excitation wavelength the response of an individual particle is the largest. This can also be observed in the large oscillations of the field created by the array. Whereas the field at the first part of the array is very large, it dies out much faster than when  $\lambda = 546$  nm is used. The reason for this is the destructive interference that may occur at certain wavelengths. It may even be the case that the decay length along the array is actually shorter than that of a single particle. In Fig. 3.15 the decay length is calculated for both an array of 50 particles and one single particle. Around  $\lambda = 450$  nm there is a crossing point, which indicates that for larger wavelengths the decay length in the array will be larger than that of a single particle.

At this point, we know how to calculate the electric field produced by an array of metal nano-particles and how to obtain criteria about the guiding properties of this array.

It remains to be shown that it is actually the SPP mode that is guided along the array. Figures 3.16 and 3.17 show the different contributions to the field produced by an array. The field is calculated on the interface, i.e. the distance to the source and the image dipole is exactly equal. Therefore, the contributions of these term are indicated by the same line. The contribution of the s-mode to the total field is very small. The reason for this is that only dipoles oscillating parallel to the interface can excite these s-polarized modes. The excitation is  $z$ -polarized and therefore, as was shown in the previous section, the  $x$ -components of the dipole moments are much smaller than the  $z$ -components. This also explains the fact that the p-modes (the SPP mode is also p-polarized) are dominating. The sharp peaks in both the SPP and the p-modes, are due to the singularity of the Hankel function at  $\rho = 0$ , as was also explained in the previous section. Again these peaks will be compensating each other. In these figures the absolute value of the electric fields are shown. In reality, however, these fields are complex valued and therefore have an amplitude and phase. Adding up the field produced by the source dipoles, the image dipoles and the s- and p-modes (without SPP), it appears that these contributions appear to be canceling. Only exactly below the dipole position a significant amount of field is left. These peaks compensate the peaks of the SPP mode. Because of the cancellation of the other contributions, the SPP mode gives the dominant contribution to the array. This result is important from the perspective of applications and computations. Since the SPP mode is a surface mode with sub-wavelength confinement, this result implies that it is very well possible to excite and guide SPPs by arrays of metal nano-particles close to a metal interface. From a computational point of view, this result is interesting, because in section 2.3.3 we showed that it is possible to analytically calculate the contribution of the SPP mode. Using this method, together with an appropriate fit to overcome the peaks at  $\rho_i = 0$  (where  $i$  indicates the particle number), it is not needed to calculate the Sommerfeld integrals for these type of systems, but a quick and analytical routine can be used.

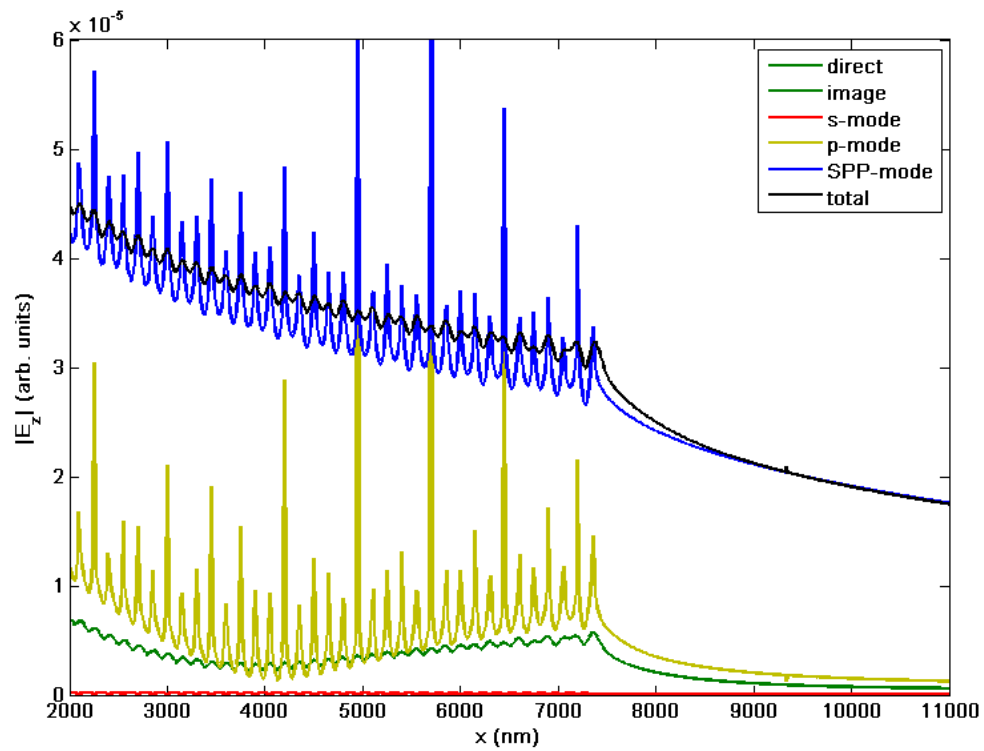


Figure 3.16: The absolute value of the  $z$ -component of the electric field produced at the interface ( $z = 0$ ) by an array of 50 silver nano-spheres ( $a = 50$  nm), with inter-particle distance of  $d = 150$  nm and a height of  $h = 150$  nm above a silver half-space. The different contributions to the total electric field are shown.

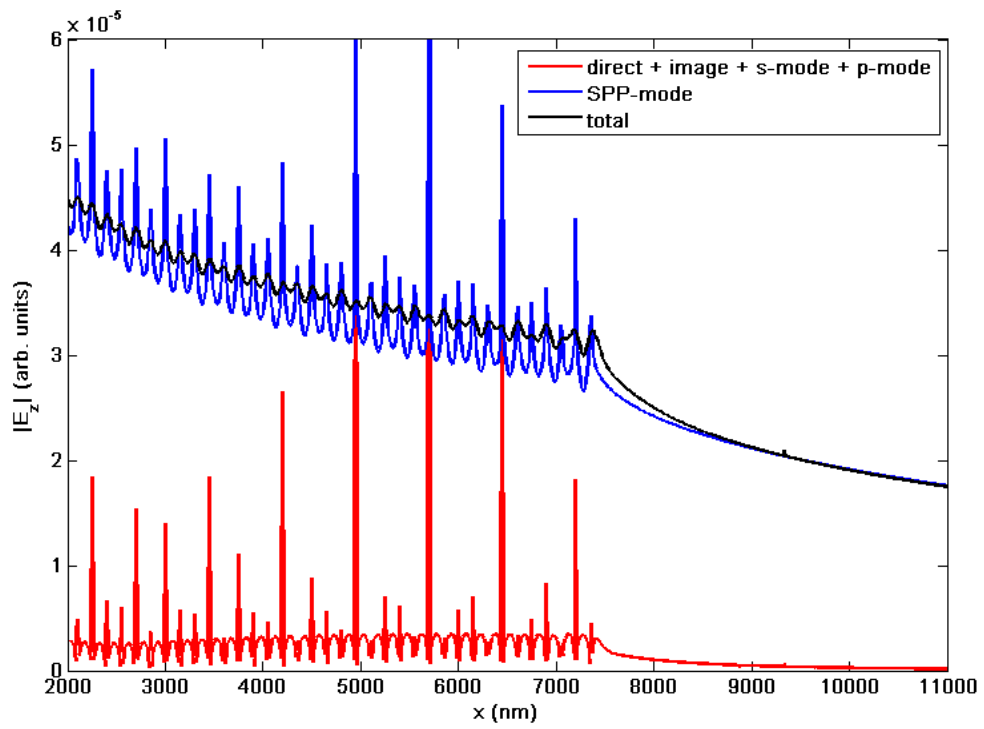


Figure 3.17: The absolute value of the  $z$ -component of the electric field produced at the interface ( $z = 0$ ) by an array of 50 silver nano-spheres ( $a = 50$  nm), with inter-particle distance of  $d = 150$  nm and a height of  $h = 150$  nm above a silver half-space. It is shown that the field corresponding to the SPPs follows the curve of the total field very closely.



## Chapter 4

# Conclusion and Suggestions for further research

In this research, three main topics have been treated: (i) the excitation of surface plasmon polariton by metal nanoparticles, (ii) energy transport through an array of metal nanoparticles in the proximity of an interface and (iii) the guiding of surface plasmon polaritons by an array of metal nanoparticles. In this concluding chapter, we will briefly write the conclusions for each topic. The final sections describes suggestions for further theoretical and experimental investigation.

### 4.1 Excitation of SPP-modes by a single Metal Nanoparticle

We showed that it is possible to excite surface plasmon polaritons on the interface between a metal and a dielectric by using the near field produced by a metal nanoparticle under continuous wave excitation. The metal nanoparticle was placed in the dielectric at a distance of 150 nm from the metal. Solving Sommerfeld integrals by making use of contour integration allowed us to separate different contributions to the electric field that is produced by the nanoparticle in such a geometry. We were able to determine the contribution of the surface plasmon modes analytically. The decay behavior of surface plasmon polaritons in this geometry is very different from the decay length that can be determined from Maxwell's equations. The reason for this is that in the latter one dimensional propagation is assumed, whereas in this system the mode will propagate in two dimensions, giving rise to an inverse square root decay of the field. For the region far away from the dipole, it

was shown that the field is almost entirely due to the SPP mode.

## **4.2 Energy transport through an array of Metal Nanoparticles in the proximity of an interface**

For determining the energy transport through an array of metal nanoparticles, we used the so-called 1% decay length of the absolute value of the dipole moments. This means that the position of the particle at which the dipole moment has decayed to 1% of the first dipole, is calculated. Using this criterion, we were able to deduce the influence of an interface close to the array. The system under consideration was an array of identical and equally spaced silver nanospheres (radius 50 nm) embedded in a dielectric medium with  $\epsilon = 2.25$ . Only the first nanosphere is excited and this was done by continuous wave irradiation.

The decay length depends very much on the excitation wavelength. Smaller center-to-center distances of the nanospheres lead to a maximum decay length that is larger (because of stronger coupling) and the excitation wavelength corresponding to this maximum shifts to the red part of the spectrum. By placing the array close to a perfect reflector, the influence of an interface was studied. In this case the interaction of the array with the 'image' array gives rise to a redshift of the maximum. Furthermore, for a separation of 150 nm between the array and the interface, the decay length is doubled with respect to the isolated array. It is interesting to note that this factor is independent of the inter-particle spacing. The reason for the increase is that part of the field that is radiated away, can be recovered via reflection at the interface. If instead of a perfect reflector we take a real metal into account (in this project we used silver), the reflected field can be calculated with the Sommerfeld integrals. These describe surface currents that are generated at the interface. One of these 'currents' corresponds to a mode propagating on the interface: the surface plasmon polariton. The presence of this mode gives rise to another increase in propagation length. However, this increase depends on how the inter-particle spacing matches with the wavelength corresponding to the SPP mode.

### 4.3 Guiding of SPP-modes by an array of Metal Nanoparticles

In the last project, the possibility to extend the propagation of the electric field by an array of metal nanoparticles was investigated. The electric field produced at the interface by a single silver nanosphere was compared to the field produced by an array of 50 nanospheres. Also in this case continuous wave excitation of the first particle was assumed.

Again the results are very much dependent on the excitation wavelength. There appears to be a critical point for which the decay lengths of the fields produced by a single particle and an array are the same. For larger wavelengths the field produced by an array has a longer decay length and therefore a longer propagation.

Finally, we showed that also in this case it is possible to separately calculate the different contributions to the electric field. As was the case for a single particle, far away from the beginning of the array the field is almost entirely plasmon like. The importance of this result is that it is possible to guide surface plasmon polariton modes by arrays of metal nanoparticles. These modes have sub-wavelength confinement and therefore this geometry allows for sub-wavelength guiding of electromagnetic fields, which is very important for applications in opto-electronics. Furthermore, the calculation of the SPP modes can be performed analytically, which implies that for these types of systems the complicated and time-taking task of calculating Sommerfeld integrals is not necessarily needed.

### 4.4 Suggestions for further research

In this project was focused on the interactions of SPPs with metal nanoparticles. One of the assumptions that might be problematic for experimental investigation, is the continuous wave excitation of only the first (sub-wavelength sized) nanosphere. However, it is important to note that in for weak excitation the response of quantum dots is exactly the same, i.e. a driven dipole oscillator. Furthermore, quantum dot can be excited electronically with high accuracy. Therefore, the research performed in this project as well as the suggestions given below can also be applied for quantum dots under electronic excitation.

In this research is was shown that it is possible to extend energy transport through a chain of metal nanoparticles, by placing the array close to a (partially) reflecting interface. Some explanation for the observed increase of propagating and shift of the maximum have

been indicated. However, in order to arrive at a full description of the important processes, it is necessary to carefully investigate the interactions between the particles in the array and that of the array with the reflected field. It was observed that the rapid decay in dipole moments is due to the near field interaction and the long tail (with small signal left) is due to the far field interactions. This makes it nontrivial to define a suitable decay criterion, which is of great importance for further investigation of this topic.

Another suggestion to further increase the SPP propagation length, is by placing the array of nanoparticles in a metal-insulator-metal waveguide. It has been shown experimentally and theoretically that if the metal layers are spaced close enough only one type of mode can fit into the waveguide, the SPP mode [27]. This implies that most of the energy inserted will be coupled to SPP modes. It has to be investigated what happens if an array of dipole emitter is placed in such a device. Important questions are how the propagation through the chain and along the interfaces will change and what the dispersion of such a propagating mode will be.

As was shown above, the electric field produced by surface plasmon polaritons can be calculated analytically and the contribution of this mode far away from the dipole (but on the interface) is large compared to the other modes present. Characterizing how large the SPP contribution to the total field is and developing a proper fitting curve to remove the peaks (see Fig. 3.17), will give a new and fast algorithm for calculating the field guided by an array of many particles close to a non-perfect reflector.

A final suggestion is based on the fact that the largest contribution to the decay of the SPP modes, is the decay over the two dimensional interface, rather than decay in one direction. If instead of a planer interface one would use e.g. a striper waveguide (metal strip on dielectric), the SPP is forced to propagate along one dimension. For the purpose of extending propagation, guiding and locally excited SPP modes, it is interesting to study the system of an array of dipole emitters on top of a striper waveguide.

## 4.5 Acknowledgements

I would like to thank Victor Malyshev and Jasper Knoester for the nice experience, the fruitful discussions and the supervision during the past year. Also, I would like to thank Javier Munarriz and Bernhard Hoenders for helping me with programming and calculating the Sommerfeld integrals.

# Appendix A

## Equations for the electric field produced by a driven dipole oscillator close to an interface

In this appendix the equations for the electric field of a dipole, embedded in medium 1, oscillating close to the interface between medium 1 and medium 2, is presented. These equations can be derived by using Sommerfelds method explained in section 2.3.

### A.1 Definitions

$E_{x,z}$	$x$ -component of the electric field produced by a dipole oscillating in the $z$ -direction
$\epsilon_i$	dielectric constant of medium $i$
$k_i$	wavevector in medium $i$
$k_r$	radial component of the wavevector at the interface
$k_{i,z}$	$\sqrt{k_i^2 - k_r^2}$ , $z$ -component of the wavevector in medium $i$
$h$	height of the dipole above the interface
$z$	vertical coordinate
$r$	$\sqrt{x^2 + y^2}$ , radial coordinate
$\theta$	radial angle, between $r$ and $x$
$R$	$\sqrt{r^2 + (z - h)^2}$ , distance between the dipole and the observation point
$R'$	$\sqrt{r^2 + (z + h)^2}$ , distance between the image dipole and the observation point
$H_\nu^{(1)}$	Hankelfunction of the first kind and of order $\nu$

## A.2 The Hertz vector potentials

The potentials in medium 1 for a dipole oscillating perpendicular (in  $z$ -direction) and parallel (in  $x$ -direction) to interface, are given by

$$\mathbf{\Pi}_{1,\perp} = \begin{pmatrix} 0 \\ 0 \\ \frac{e^{ikR}}{R} + \frac{e^{ikR'}}{R'} - 2i \int_0^\infty J_0(k\rho\rho) \frac{k_\rho}{k_{1,z}} \frac{\epsilon_1 k_{2,z}}{\epsilon_1 k_{2,z} + \epsilon_2 k_{1,z}} e^{ik_{1,z}(z+h)} dk_\rho \end{pmatrix} \quad (\text{A.2.1})$$

$$\mathbf{\Pi}_{1,\parallel} = \begin{pmatrix} \frac{e^{ikR}}{R} - \frac{e^{ikR'}}{R'} + 2i \int_0^\infty J_0(k\rho\rho) \frac{k_\rho}{k_{1,z} + k_{2,z}} e^{ik_{1,z}(z+h)} dk_\rho \\ 0 \\ -\frac{2}{k_1^2} \cos \phi \int_0^\infty J_1(k\rho\rho) \frac{\epsilon_1(k_{1,z} - k_{2,z})}{\epsilon_1 k_{2,z} + \epsilon_2 k_{1,z}} k_\rho^2 e^{ik_{1,z}(z+h)} dk_\rho \end{pmatrix} \quad (\text{A.2.2})$$

The potentials in medium 2, created by a dipole oscillating in medium 1 are

$$\mathbf{\Pi}_{2,\perp} = \begin{pmatrix} 0 \\ 0 \\ 2i \int_0^\infty J_0(k\rho\rho) \frac{k_\rho}{k_{1,z}} \frac{\epsilon_1 k_\rho}{\epsilon_1 k_{2,z} + \epsilon_2 k_{1,z}} e^{-ik_{2,z}z + ik_{1,z}h} dk_\rho \end{pmatrix} \quad (\text{A.2.3})$$

$$\mathbf{\Pi}_{2,\parallel} = \begin{pmatrix} 2i \frac{\epsilon_1}{\epsilon_2} \int_0^\infty J_0(k\rho\rho) \frac{k_\rho}{k_{1,z} + k_{2,z}} e^{-ik_{2,z}z + ik_{1,z}h} dk_\rho \\ 0 \\ -\frac{2}{k_2^2} \cos \phi \int_0^\infty J_1(k\rho\rho) k_\rho^2 \frac{\epsilon_1(k_{1,z} - k_{2,z})}{\epsilon_1 k_{2,z} + \epsilon_2 k_{1,z}} e^{-ik_{2,z}z + ik_{1,z}h} dk_\rho \end{pmatrix} \quad (\text{A.2.4})$$

Note that in this derivation, the  $x$ -component is chosen as the parallel component. Of course, the exact same procedure can be followed for the  $y$ -direction, because the cylindrical symmetry. From these Hertz vector potentials, the electric field in medium  $j$  can be calculated using the following relation

$$\mathbf{E} = \frac{1}{\epsilon_j} [k_j^2 \mathbf{\Pi}_j + \nabla(\nabla \cdot \mathbf{\Pi}_j)], \quad j = 1, 2. \quad (\text{A.2.5})$$

In the next sections, the electric field components for a dipole oscillating in the  $x$ -,  $y$ - and  $z$ -direction. For convenience, the substitution

$$J_n(z) = \frac{1}{2} [H_n^{(1)}(z) + H_n^{(2)}(z)], \quad (\text{A.2.6})$$

needed for the contour integration is already performed.

## A.3 Dipole oscillating perpendicular to the interface

$$\begin{aligned}
\vec{E}_{x,z} = & \frac{1}{\epsilon_1} \cos \theta \left[ \frac{r(3 - 3ik_1 - k_1^2 R^2)(z - h)}{R^4} \frac{e^{ik_1 R}}{R} \right. \\
& + \frac{r(3 - 3ik_1 R' - k_1^2 R'^2)(z + h)}{R'^4} \frac{e^{ik_1 R'}}{R'} \\
& \left. - \int_{-\infty}^{\infty} H_1^{(1)}(k_r r) \frac{\epsilon_1 k_{2,z}}{\epsilon_1 k_{2,z} + \epsilon_2 k_{1,z}} e^{ik_{1,z}(z+h)} k_r^2 dk_r \right]
\end{aligned} \tag{A.3.1}$$

$$\begin{aligned}
\vec{E}_{y,z} = & \frac{1}{\epsilon_1} \sin \theta \left[ \frac{r(3 - 3ik_1 - k_1^2 R^2)(z - h)}{R^4} \frac{e^{ik_1 R}}{R} \right. \\
& + \frac{r(3 - 3ik_1 R' - k_1^2 R'^2)(z + h)}{R'^4} \frac{e^{ik_1 R'}}{R'} \\
& \left. - \int_{-\infty}^{\infty} H_1^{(1)}(k_r r) \frac{\epsilon_1 k_{2,z}}{\epsilon_1 k_{2,z} + \epsilon_2 k_{1,z}} e^{ik_{1,z}(z+h)} k_r^2 dk_r \right]
\end{aligned} \tag{A.3.2}$$

$$\begin{aligned}
E_{z,z} = & \frac{1}{\epsilon_1} \left[ \left( \frac{k_1^2}{R} + \frac{ik_1}{R^2} + \frac{(3 - 3ik_1 R - k_1^2 R^2)(z - h)^2 - R^2}{R^5} \right) e^{ik_1 R} \right. \\
& + \left( \frac{k_1^2}{R'} + \frac{ik_1}{R'^2} + \frac{(3 - 3ik_1 R' - k_1^2 R'^2)(z + h)^2 - R'^2}{R'^5} \right) e^{ik_1 R'} \\
& \left. - 2i \int_{-\infty}^{\infty} H_0(k_\rho \rho) \frac{k_\rho^3}{k_{1,z}} \frac{\epsilon_1 k_{2,z}}{\epsilon_1 k_{2,z} + \epsilon_2 k_{1,z}} e^{ik_{1,z}(z+h)} dk_\rho \right]
\end{aligned} \tag{A.3.3}$$

## A.4 Dipole oscillating parallel to the interface in the x-direction

$$\begin{aligned}
\vec{E}_{x,x} = & \frac{1}{\epsilon_1} \left[ \left( k_1^2 + \frac{(3 - 3ik_1R - k_1^2R^2)x^2 + ik_1R^3 - R^2}{R^4} \right) \frac{e^{ik_1R}}{R} - \right. \\
& \left. \left( k_1^2 + \frac{(3 - 3ik_1R' - k_1^2R'^2)x^2 + ik_1R'^3 - R'^2}{R'^4} \right) \frac{e^{ik_1R'}}{R'} \right. \\
& + \frac{2i}{r} \int_{-\infty}^{\infty} \left[ \frac{r}{k_r} (k_1^2 - k_r^2 \cos^2(\theta)) H_0^{(1)}(k_r r) + (2 \cos^2(\theta) - 1) H_1^{(1)}(k_r r) \right] e^{ik_{1,z}(z+h)} \frac{k_r^2 dk_r}{k_{1,z} + k_{2,z}} \\
& \left. + \frac{i}{k_1^2 r} \int_{-\infty}^{\infty} [(2 \cos^2(\theta) - 1) H_1^{(1)}(k_r r) - rk_r \cos^2(\theta) H_0^{(1)}(k_r r)] e^{ik_{1,z}(z+h)} \frac{\epsilon_1 k_{1,z} (k_{1,z} - k_{2,z})}{\epsilon_1 k_{2,z} + \epsilon_2 k_{1,z}} k_r^2 dk_r \right]
\end{aligned} \tag{A.4.1}$$

$$\begin{aligned}
\vec{E}_{y,x} = & \frac{1}{\epsilon_1} \left[ \frac{(3 - 3ik_1R - k_1^2R^2)xy}{R^4} \frac{e^{ik_1R}}{R} - \frac{(3 - 3ik_1R' - k_1^2R'^2)xy}{R'^4} \frac{e^{ik_1R'}}{R'} \right. \\
& + \frac{i \sin \theta \cos \theta}{r^2} \int_{-\infty}^{\infty} \left[ \frac{2}{r} H_1^{(1)}(k_r r) - k_r H_0^{(1)}(k_r r) \right] e^{ik_{1,z}(z+h)} \frac{k_r^2 dk_r}{k_{1,z} + k_{2,z}} \\
& \left. + \frac{i \sin \theta \cos \theta}{k_1^2 r^2} \int_{-\infty}^{\infty} \left[ \frac{2}{r} H_1^{(1)}(k_r r) - k_r H_0^{(1)}(k_r r) \right] e^{ik_{1,z}(z+h)} \frac{\epsilon_1 k_{1,z} (k_{1,z} - k_{2,z})}{\epsilon_1 k_{2,z} + \epsilon_2 k_{1,z}} k_r^2 dk_r \right]
\end{aligned} \tag{A.4.2}$$

$$\begin{aligned}
\vec{E}_{z,x} = & \frac{1}{\epsilon_1} \left[ \frac{(3 - 3ik_1R - k_1^2R^2)(z-h)x}{R^4} \frac{e^{ik_1R}}{R} - \frac{(3 - 3ik_1R' - k_1^2R'^2)(z+h)x}{R'^4} \frac{e^{ik_1R'}}{R'} \right. \\
& + \cos \theta \int_{-\infty}^{\infty} H_1^{(1)}(k_r r) e^{ik_{1,z}(z+h)} \frac{k_{1,z} k_r^2 dk_r}{k_{1,z} + k_{2,z}} \\
& \left. + \cos \theta \int_{-\infty}^{\infty} H_1^{(1)}(k_r r) e^{ik_{1,z}(z+h)} \frac{\epsilon_1 (k_{1,z} - k_{2,z})}{\epsilon_1 k_{2,z} + \epsilon_2 k_{1,z}} k_r^2 dk_r \right]
\end{aligned} \tag{A.4.3}$$



## A.5 Dipole oscillating parallel to the interface in the y-direction

$$\begin{aligned}
\vec{E}_{x,y} = & \frac{1}{\epsilon_1} \left[ \frac{(3 - 3ik_1R - k_1^2R^2)xy e^{ik_1R}}{R^4} - \frac{(3 - 3ik_1R' - k_1^2R'^2)xy e^{ik_1R'}}{R'^4} \frac{1}{R} \right. \\
& + \frac{i \sin \theta \cos \theta}{r^2} \int_{-\infty}^{\infty} \left[ \frac{2}{r} H_1^{(1)}(k_r r) - k_r H_0^{(1)}(k_r r) \right] e^{ik_{1,z}(z+h)} \frac{k_r^2 dk_r}{k_{1,z} + k_{2,z}} \\
& \left. + \frac{i \sin \theta \cos \theta}{k_1^2 r^2} \int_{-\infty}^{\infty} \left[ \frac{2}{r} H_1^{(1)}(k_r r) - k_r H_0^{(1)}(k_r r) \right] e^{ik_{1,z}(z+h)} \frac{\epsilon_1 k_{1,z} (k_{1,z} - k_{2,z})}{\epsilon_1 k_{2,z} + \epsilon_2 k_{1,z}} k_r^2 dk_r \right]
\end{aligned} \tag{A.5.1}$$

$$\begin{aligned}
\vec{E}_{y,y} = & \frac{1}{\epsilon_1} \left[ \left( k_1^2 + \frac{(3 - 3ik_1R - k_1^2R^2)y^2 + ik_1R^3 - R^2}{R^4} \right) \frac{e^{ik_1R}}{R} - \right. \\
& \left( k_1^2 + \frac{(3 - 3ik_1R' - k_1^2R'^2)y^2 + ik_1R'^3 - R'^2}{R'^4} \right) \frac{e^{ik_1R'}}{R'} \\
& + \frac{2i}{r} \int_{-\infty}^{\infty} \left[ \frac{r}{k_r} (k_1^2 - k_r^2 \sin^2(\theta)) H_0^{(1)}(k_r r) + (2 \sin^2(\theta) - 1) H_1^{(1)}(k_r r) \right] e^{ik_{1,z}(z+h)} \frac{k_r^2 dk_r}{k_{1,z} + k_{2,z}} \\
& \left. + \frac{i}{k_1^2 r} \int_{-\infty}^{\infty} \left[ (2 \sin^2(\theta) - 1) H_1^{(1)}(k_r r) - r k_r \sin^2(\theta) H_0^{(1)}(k_r r) \right] e^{ik_{1,z}(z+h)} \frac{\epsilon_1 k_{1,z} (k_{1,z} - k_{2,z})}{\epsilon_1 k_{2,z} + \epsilon_2 k_{1,z}} k_r^2 dk_r \right]
\end{aligned} \tag{A.5.2}$$

$$\begin{aligned}
\vec{E}_{z,y} = & \frac{1}{\epsilon_1} \left[ \frac{(3 - 3ik_1R - k_1^2R^2)(z - h)y e^{ik_1R}}{R^4} - \frac{(3 - 3ik_1R' - k_1^2R'^2)(z + h)y e^{ik_1R'}}{R'^4} \frac{1}{R} \right. \\
& + \sin \theta \int_{-\infty}^{\infty} H_1^{(1)}(k_r r) e^{ik_{1,z}(z+h)} \frac{k_{1,z} k_r^2 dk_r}{k_{1,z} + k_{2,z}} \\
& \left. + \sin \theta \int_{-\infty}^{\infty} H_1^{(1)}(k_r r) e^{ik_{1,z}(z+h)} \frac{\epsilon_1 (k_{1,z} - k_{2,z})}{\epsilon_1 k_{2,z} + \epsilon_2 k_{1,z}} k_r^2 dk_r \right]
\end{aligned} \tag{A.5.3}$$

# Bibliography

- [1] S. A. Maier. Plasmonics: Fundamentals and Applications, Springer, (2008).
- [2] L. Novotny, B. Hecht. Principles of Nano-Optics, 1st edition, Cambridge University Press (2008).
- [3] G. Mie. Beiträge zur Optik trüber Medien, speziell kolloidaler Metallösungen. *Ann. Phys. Vierte Folge* **25**, 377 (1908).
- [4] C. F. Bohren, D. R. Huffman. Absorption and Scattering of Light by Small Particles, Wiley Science (1982).
- [5] S. A. Maier, H. A. Atwater. Plasmonics: Localization and guiding of electromagnetic energy in metal/dielectric structures. *J. Appl. Phys.* **98**, 011101 (2005).
- [6] E. Ozbay. Plasmonics: Merging Photonics and Electronics at Nanoscale Dimensions. *Science* **311**, 189 (2006).
- [7] R. de Waele, A. F. Koenderink, A. Polman. Tunable Nanoscale Localization of Energy on Plasmon Particle Arrays. *Nano Lett.* **7**, 2004 (2007)
- [8] H. A. Atwater, A. Polman. Plasmonics for improved photovoltaic devices. *Nat. Materials* **9**, 205 (2010)
- [9] L. Novotny, N. van der Hulst. Antennas for light. *Nat. Photonics* **5**, 83 (2011)
- [10] M. Quinten, A. Leitner, R. M. Krenn, F. R. Aussenegg. Electromagnetic energy transport via linear chains of silver nanoparticles. *Opt. Lett.* **23**, 1331 (1998).
- [11] A. B. Evlyukhin and S. I. Bozhevolnyi. Surface plasmon polariton guiding by chains of nanoparticles. *Laser Phys. Lett.* **3**, 8, 396-400 (2006).
- [12] A. V. Malyshev, V. A. Malyshev, J. Knoester. Frequency-Controlled Localization of Optical Signals in Graded Plasmonic Chains. *Nano Lett.* **8**, 2369 (2008).
- [13] M. L. Brongersma, J. W. Hartman, H. A. Atwater. Electromagnetic energy transfer and switching in nanoparticle chain arrays below the diffraction limit. *Phys. Rev. B* **62**, R16356 (2000).

- 
- [14] A. Sommerfeld. Über die Ausbreitung der Wellen in der drahtlosen Telegraphie. *Ann. Phys. Vierte Folge* **28**, 665 (1909).
- [15] J. Zenneck. Über die Fortpflanzung ebener elektromagnetischer Wellen längs einer ebenen Leiterfläche und ihre Beziehung zur drahtlosen Telegraphie. *Ann. Phys.* **23**, 846 (1907)
- [16] J. A. Dionne, L. A. Sweatlock, H. A. Atwater, A. Polman. Plasmon slot waveguides: Towards chip-scale propagation with subwavelength-scale localization. *Phys. Rev. B* **73**, 035407 (2006)
- [17] R. J. Walters, R. V. A. van Loon, I. Brunets, J. Schmitz, A. Polman. A silicon-based electrical source of surface plasmon polaritons. *Nat. Materials Lett.* **2595** (2009).
- [18] M. Meier, A. Wokaun. Enhanced fields on large metal particles: dynamic depolarization. *Opt. Lett.* **8**, 581 (1983)
- [19] J. D. Jackson. *Classical Electrodynamics*, 3rd edition, Wiley (1999).
- [20] E. Wolf, M. Nieto-Vesperinas. Analyticity of the angular spectrum amplitude of scattered fields and some of its consequences. *J. Opt. Soc. Am. A* **2**, 886, (1985)
- [21] A. Sommerfeld. *Partial Differential Equations in Physics*, Academic Press (1964)
- [22] H. Hertz. Die Kräfte elektrischer Schwindungen. *Ann. Phys. u. Chem.* **1** (1889)
- [23] M. Paulus, P. Gay-Balmaz, O. J. F. Martin. Accurate and efficient computation of the Green's tensor for stratified media, *Phys. Rev. E* **62**, 4 (2000).
- [24] R. R. Chance, A. Prock, R. Silbey. Molecular fluorescence and energy transfer near interfaces. *Adv. Chem. Phys.* (1978).
- [25] W. L. Barnes. Fluorescence near interfaces: the role of photonic mode density. *J. Modern Optics* **45**, 4 (1998)
- [26] M. Abramowitz, I. A. Stegun. *Handbook of Mathematical Functions*, Dover (1972).
- [27] Y. C. Jun, R. D. Kekatpure, J. S. White, and M. L. Brongersma. Nonresonant enhancement of spontaneous emission in metal-dielectric-metal plasmon waveguide structures. *Phys. Rev. B* **78**, 153111 (2008)